AL-TR-90-049 AD:

(2)

Final Report
for the period
April 1987 to
June 1990

Ionic Solid Hydrogen Fuel : Production and Properties of Hydrogen Ion and Energetic Neutral Clusters

September 1990

Author:
Young K. Bae
Philip C. Cosby

SRI International
333 Ravenswood Avenue
Menlo Park CA 94025

F04611-87-C-0025
MP 90-080

Approved for Public Release

Distribution is unlimited. The AL Technical Services Office has reviewed this report, and it is releasable to the National Technical Information Service, where it will be available to the general public, including foreign nationals.

Prepared for the: **Astronautics Laboratory (AFSC)**
Air Force Space Technology Center
Space Systems Division
Air Force Systems Command
Edwards AFB CA 93523-5000

NOTICE

When U. S. Government drawings, specifications, or other data are used for any purpose other than a definitely related Government procurement operation, the fact that the Government may have formulated, furnished, or in any way supplied the said drawings, specifications, or other data, is not to be regarded by implication or otherwise, or in any way licensing the holder or any other person or corporation, or conveying any rights or permission to manufacture, use or sell any patented invention that may be related thereto.

FOREWORD

This final report was submitted by Molecular Physics Laboratory, Menlo Park CA on completion of contract F04611-87-C-0025 with the Astronautics Laboratory (AFSC), Edwards AFB CA. AL Project Manager is Capt Tim Wiley.

This report has been reviewed and is approved for release and distribution in accordance with the distribution statement on the cover and on the DD Form 1473.

Stephen L. Rodgers

TIMOTHY G. WILEY, CAPT, USAF
Project Manager

STEPHEN L. RODGERS
Chief, Applied Research in Energy Storage Office

FOR THE DIRECTOR

Robert C. Corley

ROBERT C. CORLEY
Director, Astronautical Sciences Division

SECURITY CLASSIFICATION OF THIS PAGE

REPORT DOCUMENTATION PAGE

Form Approved OMB No. 0704-0188

1a. REPORT SECURITY CLASSIFICATION: UNCLASSIFIED	1b. RESTRICTIVE MARKINGS
2a. SECURITY CLASSIFICATION AUTHORITY	3. DISTRIBUTION/AVAILABILITY OF REPORT: Approved for Public Release; Distribution is Unlimited
2b. DECLASSIFICATION/DOWNGRADING SCHEDULE	
4. PERFORMING ORGANIZATION REPORT NUMBER(S): MP 90-080	5. MONITORING ORGANIZATION REPORT NUMBER(S): AL-TR-90-049
6a. NAME OF PERFORMING ORGANIZATION: Molecular Physics Laboratory; 6b. OFFICE SYMBOL (If applicable):	7a. NAME OF MONITORING ORGANIZATION: Astronautics Laboratory (AFSC)
6c. ADDRESS (City, State, and ZIP Code): SRI International, 333 Ravenswood Avenue, Menlo Park CA 94025	7b. ADDRESS (City, State, and ZIP Code): AL/LSX, Edwards AFB CA 93523-5000
8a. NAME OF FUNDING/SPONSORING ORGANIZATION; 8b. OFFICE SYMBOL (If applicable):	9. PROCUREMENT INSTRUMENT IDENTIFICATION NUMBER: F04611-87-C-0025
8c. ADDRESS (City, State, and ZIP Code)	10. SOURCE OF FUNDING NUMBERS

PROGRAM ELEMENT NO.	PROJECT NO.	TASK NO	WORK UNIT ACCESSION NO.
62302F	5730	008H	344000

11. TITLE (Include Security Classification): Ionic Solid Hydrogen Fuel: Production and Properties of Hydrogen Ion and Energetic Neutral Clusters (U)

12. PERSONAL AUTHOR(S): Bae, Young K., and Cosby, Philip C.

13a. TYPE OF REPORT	13b. TIME COVERED	14. DATE OF REPORT (Year, Month, Day)	15. PAGE COUNT
Final	FROM 8704 TO 9006	9009	84

16. SUPPLEMENTARY NOTATION

17. COSATI CODES			18. SUBJECT TERMS (Continue on reverse if necessary and identify by block number)
FIELD	GROUP	SUB-GROUP	matrix, hydrogen, cluster, cluster ion, hydrogen matrix, cluster beams
19	07		
21	09		

19. ABSTRACT (Continue on reverse if necessary and identify by block number)

We have demonstrated that the production of intense beams of positive hydrogen cluster ions is quite feasible, and should allow their rapid embedment in a H_2 matrix. However, stabilization of these species by codeposition of hydrogen cluster anions does not appear to be a useful approach, because of the extreme difficulty we have encountered in generating the negative hydrogen cluster beams. One approach which has not been investigated is to generate the stabilizing anion directly within the matrix. Whereas the hydrogen anion clusters may be unstable in the gas phase, within the matrix H^- may form a cavity by repelling the surrounding H_2 molecules to produce a locally stable structure.

A much more promising way of achieving an extremely high energy density for rocket propulsion is the use of hydrogen-containing cluster ions for igniting nuclear fusion (cluster-impact fusion, CIF). The energy density that can be achieved by CIF with the DT fuel is 3.4×10^{14} J/kg which is eight orders of magnitude larger than the energy density of LOX/H_2 (1.6×10^6 J/kg). For missions with $I_{sp}<10^5$ s, the CIF rocket performance will be essentially identical to that of antimatter. However, production and storage of CIF fuels will be straightforward, because it uses regular matter instead of antimatter. Under the current project, we have developed new high intensity cluster ion sources which are essential for CIF experiments. Furthermore, we have added additional apparatuses, including a 300-kV electrostatic accelerator, to the existing cluster facility with the construction partly supported by the current project.

20. DISTRIBUTION/AVAILABILITY OF ABSTRACT	21. ABSTRACT SECURITY CLASSIFICATION	
☐ UNCLASSIFIED/UNLIMITED ☐ SAME AS RPT ☐ DTIC USERS	UNCLASSIFIED	
22a. NAME OF RESPONSIBLE INDIVIDUAL: TIMOTHY G. WILEY, CAPTAIN, USAF	22b. TELEPHONE (Include Area Code): (805) 275-5749	22c. OFFICE SYMBOL: LSX

DD Form 1473, JUN 86 — Previous editions are obsolete. — SECURITY CLASSIFICATION OF THIS PAGE

CONTENTS

INTRODUCTION AND SUMMARY

SRI International (SRI) is pleased to present this final report to the Astronautics Laboratory (AFSC) under Contract FO4611-87-C-0025, on the subject of ionic solid hydrogen fuel. A new high energy density material for advanced propulsion systems should have high energy content, low weight combustion products, and a long enough lifetime that it can be stored safely during the interval between production and use. Three years ago we proposed storage of stable positive and negative ions separately in a hydrogen matrix (ionic solid hydrogen). The ionic solid hydrogen may satisfy these requirements for an advanced propulsion fuel because:

(1) The positive and negative ion pairs have the highest energy content among chemical species, and, if they can be separately trapped in a matrix, they are stable.

(2) Among matrices, the hydrogen matrix is the only one that promises to yield a higher specific impulse I_{sp} than the benchmark $H_2 + O_2$ system.

Figure 1 shows the approximate I_{sp} of ionic solid hydrogen containing H_3^+ and H^- ions as a function of ion molar concentration. With a molar concentration of 2%, the specific impulse I_{sp} is over 600 s. With a molar concentration of up to 5%, switching from hydrogen ions to other light ions does not change the I_{sp} significantly.

When the ions are created and imbedded in a hydrogen matrix, their properties significantly change from those in the gas phase, and they are expected to form ion cluster structures locally, if they are sufficiently isolated from each other. The local binding force of the cluster ions forms a barrier against the long range attractive Coulomb force between the isolated ions. Furthermore, the clustered hydrogen molecules shield the core ion charge, decreasing the Coulomb force seen by the oppositely charged ions. Thus, stability of the ionic solid hydrogen depends on the geometry of the ions and their potential for binding to the surrounding matrix molecules; the structure and properties of the hydrogenic ion clusters themselves.

Which ions are the most stable in a hydrogen matrix? What is the maximum density of ion storage? What is the optimum method for producing such a fuel? For three years, we have worked to illuminate these questions by systematically studying cold cluster ions as they grow from simple ionic cores to clusters. Especially we have been trying to identify and characterize the first-occuring, completely closed shell structures of clusters that are likely to have high stability in the matrix environment.

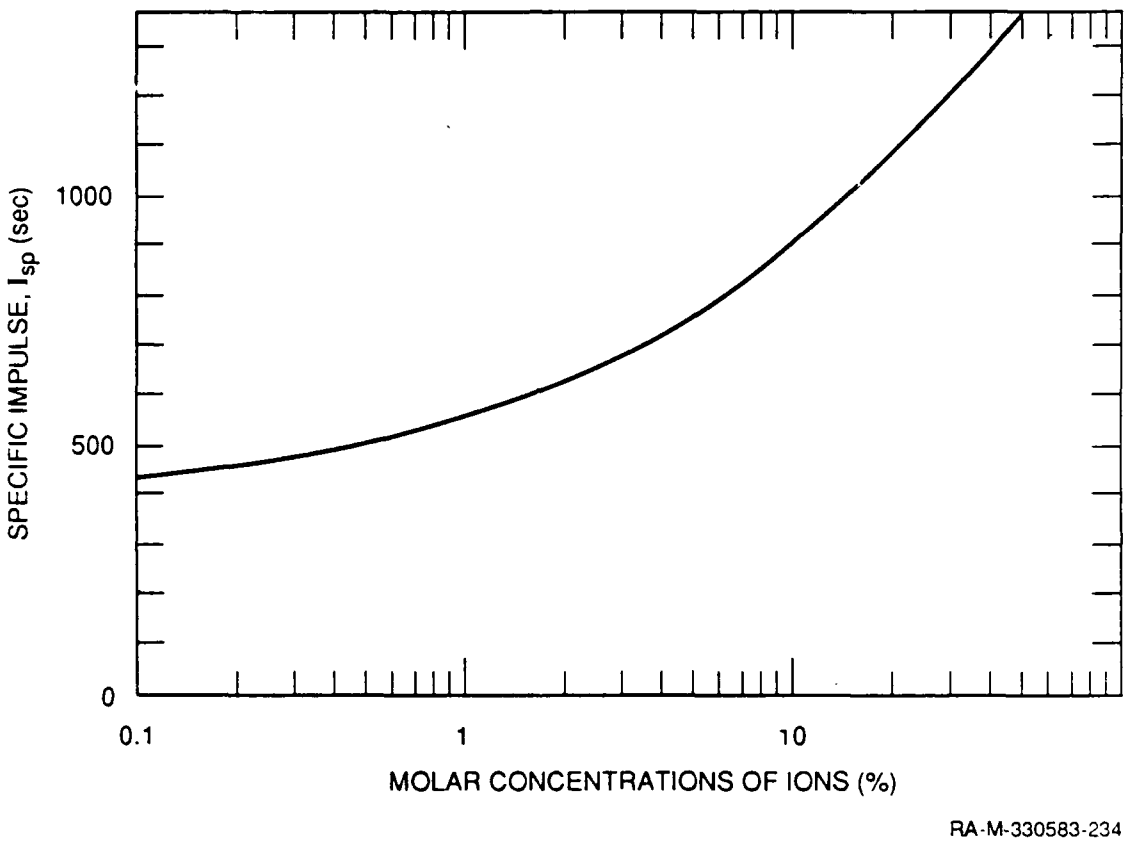

Figure 1. Approximate specific impulse of the ionic solid hydrogen as a function of H_3^+ and H^- ion molar concentration.

From our cluster ion study[1] along with other studies[2,3] we may conclude that when H_3^+ ions are imbedded or H_2 molecules are ionized in a hydrogen matrix, they form the stable closed H_{27}^+ cluster ions with possibly a linear H_7^+ core. Thus, stable embedment of positive ions, especially H_3^+, seems relatively straightforward. However, stable embedment of counter negative ions, especially H^-, in a hydrogen matrix seems nontrivial because hydrogen negative ions in the gas phase are not stable.[4] In a matrix, however, H^- might form a cavity by repelling the surrounding H_2 molecules to form a locally stable structure.[5] Therefore, we may conclude that the stable embedment of H_3^+ and H^- may be feasible, if their densities are not too high. The maximum storable densities and lifetimes of these ions are subjects of future investigation.

The use of cluster ions to simulate matrix effects allows the applications of powerful spectroscopic diagnostics not practical in matrix study alone. We measured photoabsorption spectra of H_3^+ and H_5^+, which are core ions for small positive hydrogen cluster ions, by monitoring photofragmentation.[6,7] We found the spectrum of H_5^+ will be especially useful to identify it in a hydrogen matrix.

Almost at the end of this project, a new application of hydrogen-containing cluster ions for nuclear fusion was discovered by Brookhaven scientists.[8] The surprising aspects of these experiments are the magnitude and energy dependence of the fusion yield. The magnitude suggests a surprisingly efficient mechanism of compression and confinement, a form of inertial confinement, as yet not understood. The extremely steep energy dependence is headed toward a break-even point at less than 1 MeV on the D-D reaction with only a 200-molecule cluster ion impacting a deuterated target. It seems that the Brookhaven scientists have discovered a new and effective mode of inertial confinement that is amenable to rapid technological development if the physics continues to be promising. The technology for developing a practical rocket engine from cluster-impact fusion could occur very quickly because large mass cluster ions can be accelerated efficiently with a well developed accelerator technology, and because cluster ion source technology is available.

In fact, nuclear fusion is a very promising way of achieving extremely high energy density materials for rocket propulsion. The anticipated performance of a rocket propulsion system based on fusion is comparable with that based on antimatter. However, the conventional fusion devices seem too bulky to be used for rocket engines; thus, new fusion schemes that promise very compact fusion devices must be sought. After carefully investigating the discovery, we concluded that cluster-impact fusion might potentially lead to a very simple, efficient, and very compact fusion rocket engine. After discussions with the technical monitor we redirected our efforts toward the

investigation of the application of CIF as a fuel for rocket propulsion. Under the current contract we are assembling additional apparatuses, including a 300 keV electrostatic accelerator in the existing cluster facility, for careful investigation of the discovery. Because cluster-impact fusion requires a very high flux of large clusters, we have developed a new a very high flux cluster ion source that can be used for generating clusters of various materials, including LiD.[9]

The remainder of this report discusses in some detail our findings; the appendices contain publications developed under this contract. A brief summary of our accomplishments and an indication of our next efforts comprise the conclusion of this report.

RESULTS

Two major tasks for achieving high energy density materials with hydrogen-containing cluster ions were performed under the present contract. The first task focused on ionic solid hydrogen and the second one on cluster-impact fusion. The following sections summarize our research efforts and results for these two tasks.

IONIC SOLID HYDROGEN

Under the present contract we built and demonstrated an experimental apparatus for the systematic study of cluster ions. The major experimental results related to ionic solid hydrogen are summarized below.

Demonstration of the High Intensity Versatile Cluster Ion Source

Spectroscopic studies of hydrogen cluster ions are essential in understanding the behavior of H_3^+ ions in a hydrogen matrix. So far only very few such studies have been performed on hydrogen cluster ions because the clusters are difficult to generate in abundance. Under the present contract, we have successfully developed and demonstrated a high intensity hydrogen cluster ion source. The principal mechanisms of the source are shown in Figure 2. The process begins with cluster ions grown around high intensity seed ions, which are generated by the electron impact ionization of H_2 molecules very near the exit of the nozzle (~1 nozzle diameter distance). Then the generated cluster ions are coaxially focussed and extracted from the pulsed (10 Hz, 200 μsec) supersonic expansion through a skimmer. The new source assembly can generate well collimated, intense beams of hydrogen cluster ions as well as various positive and negative cluster ions, such as H_3O^+, $(CO)_n^+$, $(NO)_n^+$, He_n^+, Ne_n^+, Ar_n^+, Xe_n^+, and $(CO_2)_n^+$ and $(CO_2)_n^-$. At a backing pressure of ~1 atmosphere in the nozzle, the intensity of the cluster ions selected by size decreases monotonically with n. For a cluster size n = 10, the source produces a peak current of 500 pA, which is sufficient for photofragment studies with a pulsed laser. We have performed a preliminary photofragmentation study with $(CO)_n^+$ cluster ions to demonstrate the capability of the source. Figure 3 shows photoabsorption spectra of $(CO)_2^+$ and $(CO)_3^+$. Since the demonstration, we have been consulting with the Astronautics Laboratory on the construction of a similar source based on our design. The details of the source and its operation are given in Appendix A.

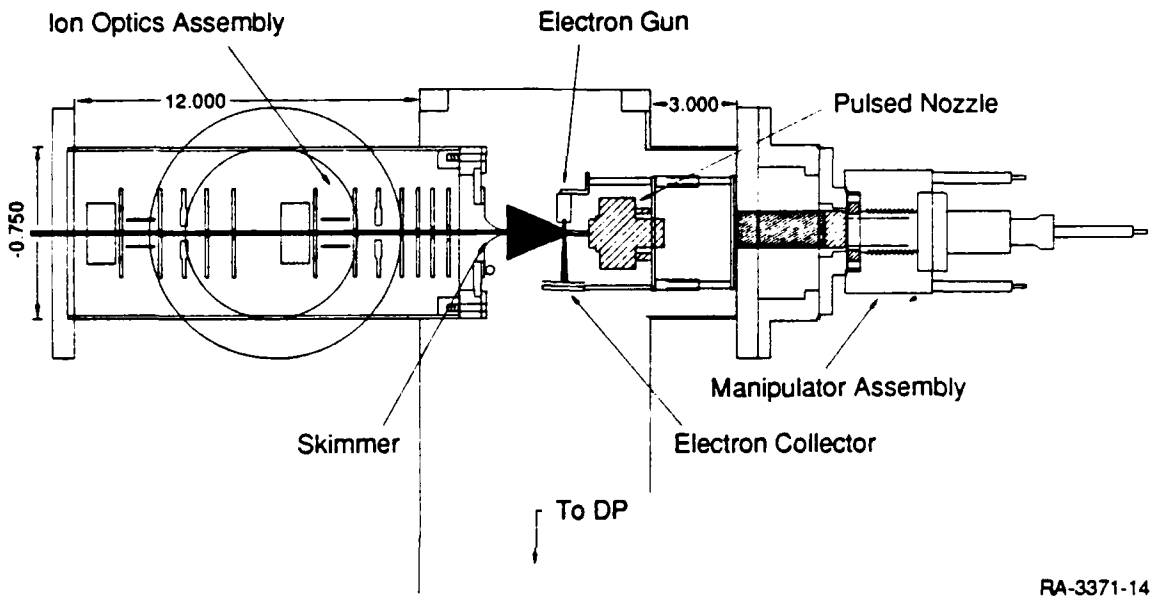

Figure 2. Schematic of the pulsed cluster ion source.

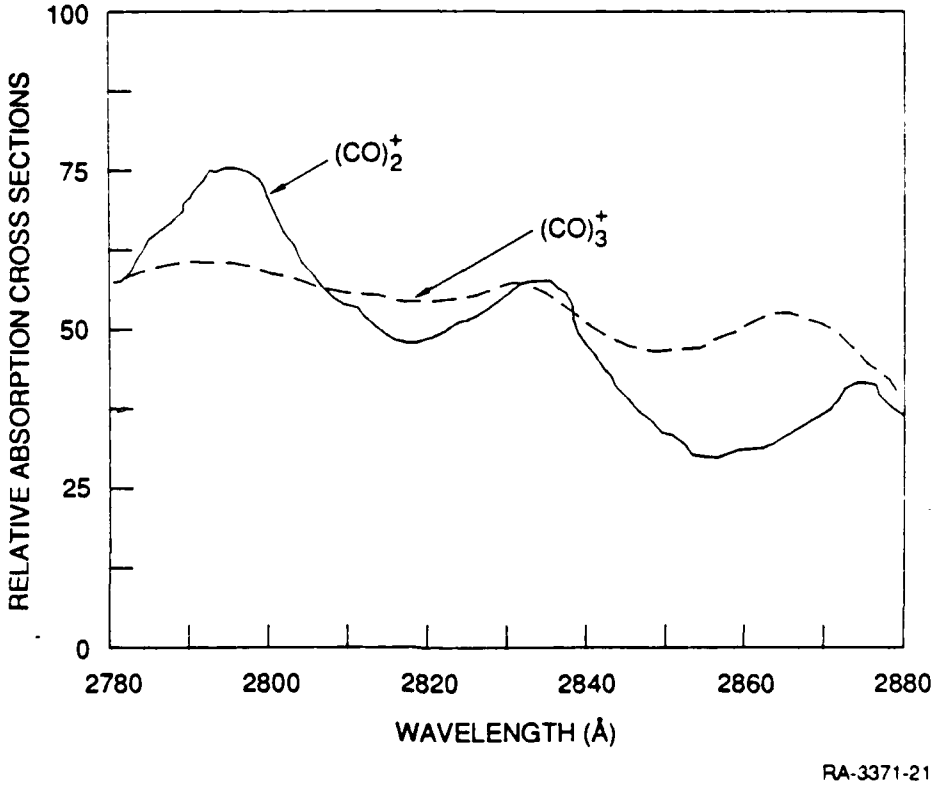

Figure 3. Photoabsorption spectra of $(CO)_2^+$ and $(CO)_3^+$.

Observation of Fivefold Symmetry in Geometric Structures of Various Cluster Ions

During our extensive investigation of the new source, we discovered shell structures manifested in the size distribution of various cluster ions.[10] It appears that fivefold symmetry is very common in the cluster ion geometrical structures. Pentagonal bipyramid structures with five neutrals surrounding a dimer ion core seem to describe $(CO)_n^+$ and $(N_2)_n^+$ cluster ions (Figure 4, Figure 5a). Elongated icosahedral structures with fivefold crowns appear to describe the Xe_n^+ cluster ion structure (Figure 6, Figure 5b). Details of these experiments and results are given in Appendix B. The results of this study helped to unravel the structures of the hydrogen cluster ions described in the next section.

Geometric Structures of H_{2n+1}^+ Cluster Ions

Current theoretical studies predict that the geometric structures of H_{2n+1}^+ cluster ions are dominated by the equilateral triangular geometry of H_3^+, and that H_{13}^+ forms a completed shell structure.[2,11] However our study[10] under this contract, along with other experimental work, indicates an unusual stability for the H_{15}^+ ion, suggesting that H_{15}^+, not H_{13}^+, should best be described by a completed shell structure.[3,12] As mentioned in the previous section, fivefold symmetry is very common in the geometric structures of nonmetallic ion clusters. Based on the fivefold symmetry, we suggest that the H_{15}^+ might be stable because it has the pentagonal bipyramid structure with the H_5^+ core ion, possibly with D_{2h} or D_{2d} geometry (Figure 7).

Furthermore, experimental results of other researchers[3] have shown that hydrogen cluster ions larger than H_{15}^+ also form stable structures. In their collisional dissociation study of hydrogen cluster ions up to H_{41}^+, van Lumig and Reuss[3] found extra stability of H_{27}^+. They also observed that H_{19}^+ and H_{23}^+ are relatively stable compared with their neighbors. We correlated the extra stability of H_{27}^+ with an icosahedron structure in which 10 H_2 molecules surround an almost linear H_7^+ core ion. We note here that a similar structure is also indicated for Xe_{13}^+, shown in Figure 5b. Assuming this picture is correct, we have unravelled the structures of all H_{2n+1}^+ cluster ions up to H_{27}^+ (Figure 7 and 8). We also note that the relative stability of H_{19}^+ and H_{23}^+ might result from their possible isomers with higher geometric symmetry, (H_7^+,3,3) and (H_7^+,4,4) respectively. The discussion of these geometric structures of hydrogen cluster ions is in Appendix C.

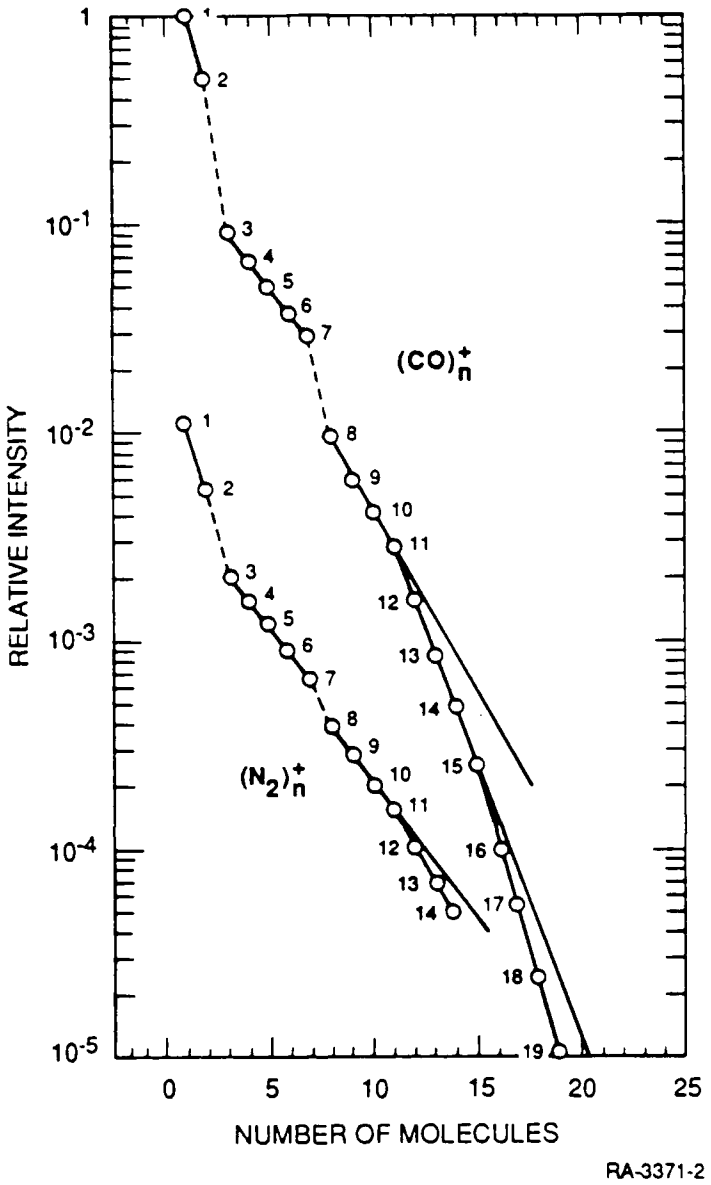

Figure 4. Intensity distribution as a function of the size of $(CO)_n^+$ and $(N_2)_n^+$ cluster ions.

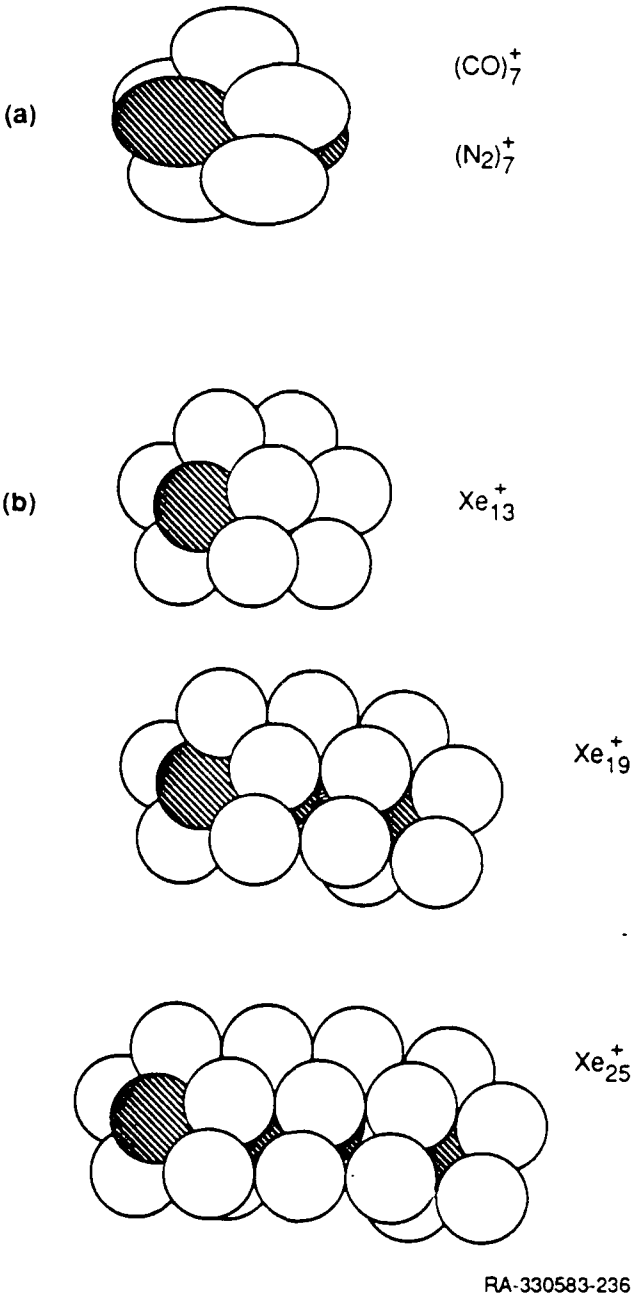

Figure 5. Proposed structures of other cluster ions.

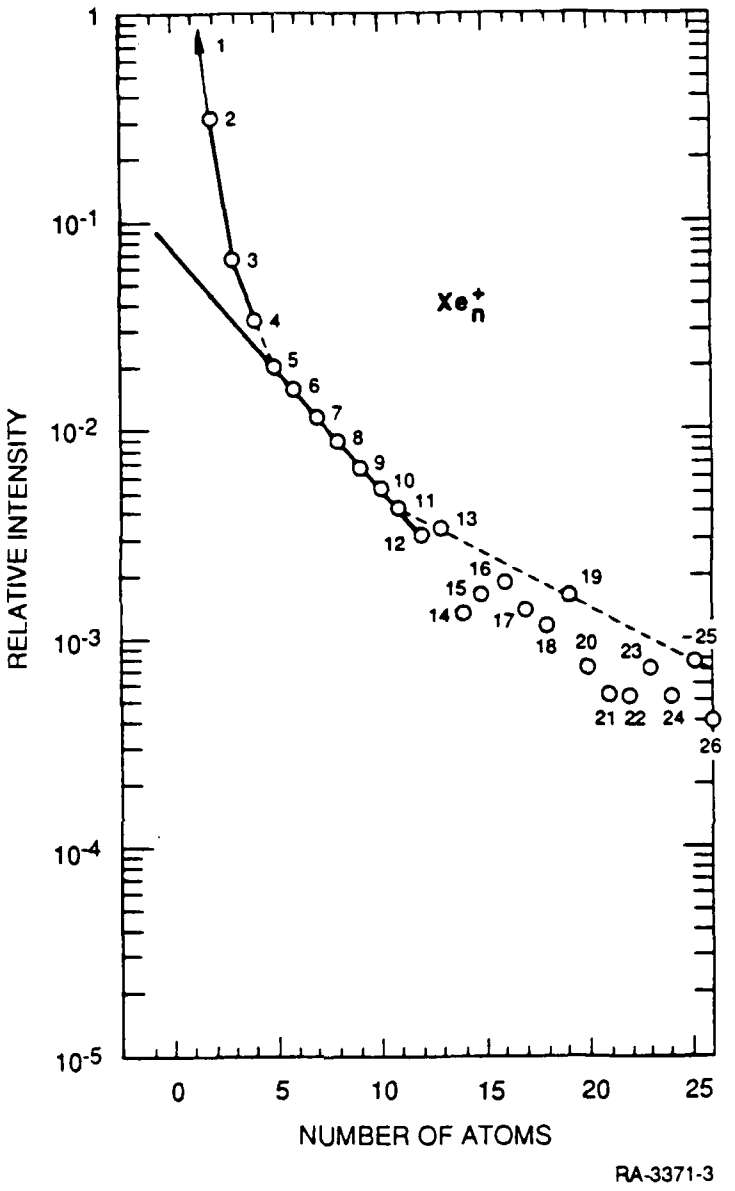

Figure 6. Intensity distribution as a function of the size of Xe_n^+ cluster ions.

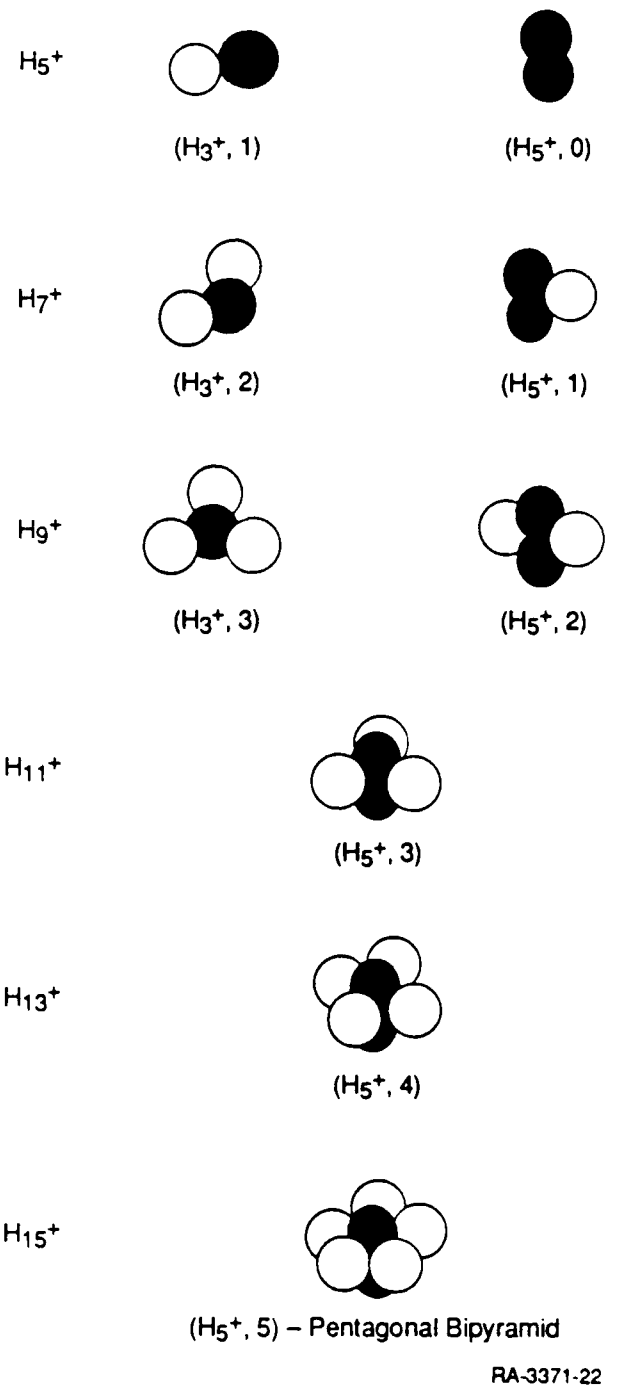

Figure 7. The proposed structures of hydrogen cluster ions.

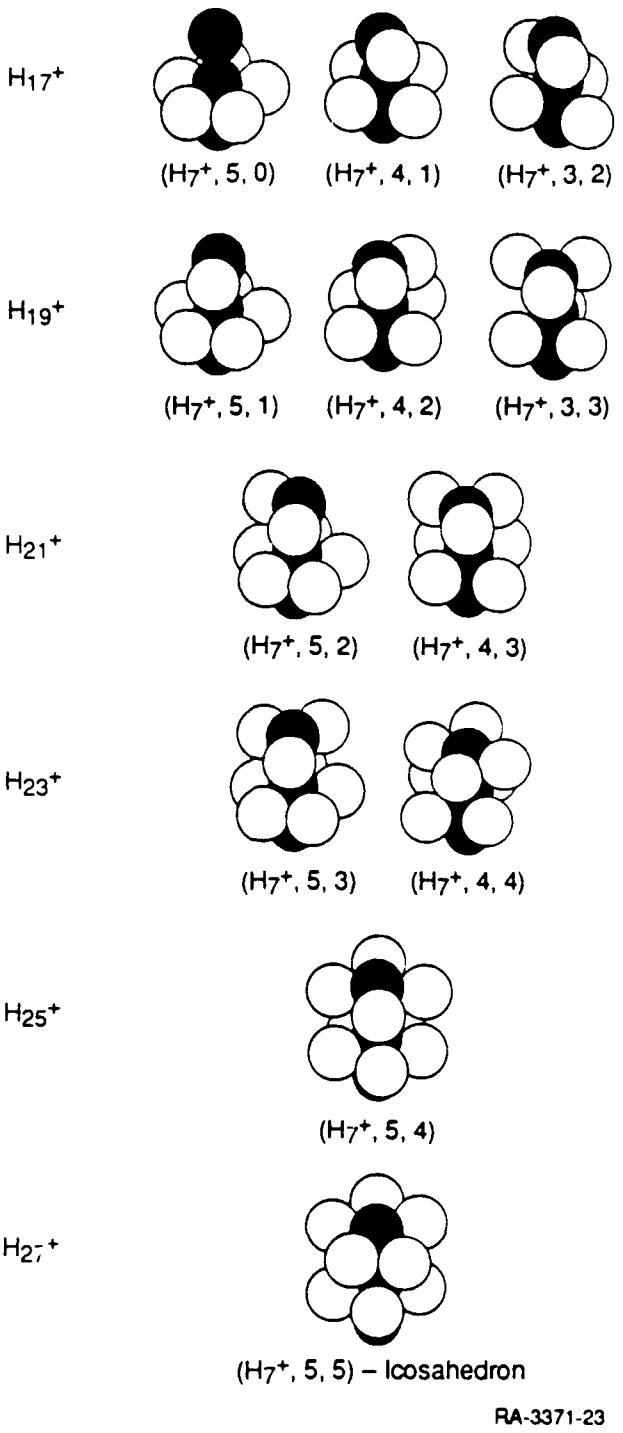

Figure 8. The proposed structures of hydrogen cluster ions.

First Observation of Direct Photodissociation of H_3^+

The H_3^+ ion plays a key role in understanding the properties of H_{2n+1}^+ cluster ions. The structure of H_3^+ and its isotopomers has been successfully probed in a variety of experiments. These experiments, however, have explored only the ground electronic state of the ion, labeled $1^1A_1'$ or $1^1A'$ in D_{3h} or C_{2v} symmetry, respectively. Other electronic states are known only from quantum chemistry calculations.[13] When accessed at the equilibrium geometry of the ground electronic state, these excited states are expected to be prohibitively high in energy for optical excitation. For many years only a single experiment, electron-impact dissociation to form protons,[14] has successively accessing any excited state of H_3^+. Under the present contract, we have successfully measured for the first time the near-threshold bound-free photodissociation of H_3^+ into $H_2^+ + H$ by observing H_2^+ photofragments. Figure 9 shows the result. The observed transition was interpreted to be the predicted direct photodissociation transition between the ground state ($1^1A'$) and the first excited state ($1^1E'$) with C_s geometry.[13] The observed threshold energy of ~2.5 eV is consistent with the theoretically predicted value.[13] The details of this study are given in Appendix D.

First Observation of High-Lying Vibrational States of H_5^+

Our work discussed in the previous sections indicates that H_5^+ is the core ion for hydrogen cluster ions larger than H_9^+ and smaller than H_{17}^+ (see Figure 7). Calculations predict a global minimum structure of H_5^+ with C_{2v} geometry which can be described by an H_2 molecule bonded to an H_3^+ core. However, other structures such as D_{2d} and D_{2h} symmetries, which can be described as $H_2 \bullet H^+ \bullet H_2$, are predicted to be nearly degenerate in energy.[15]

Okumura et al.[16] measured a photodissociation spectrum of H_5^+ between 3000 and 5300 cm^{-1}, and observed three vibrational transitions of the H_5^+ in the region of 4000 cm^{-1}. The first portion of Table 1 summarizes their results and assignments. The two transitions were confidently identified with the ν_1 and ν_2 modes on the basis of the calculated harmonic frequencies for the global minimum C_{2v} structure of H_5^+. Here ν_1 and ν_2 are the vibrational mode of H_2 and the symmetric stretch mode of H_3^+ in H_5^+, respectively. The other mode was assigned to be either $\nu_1 + \nu_8$ or $3\nu_4$. Here ν_4 and ν_8 are the asymmetric stretch mode of H_3^+ and the intermolecular stretch mode between H_3^+ and H_2 in H_5^+, respectively. Under this contract, we measured the spectrum between 5400 and 10000 cm^{-1}, and observed for the first time four more transitions near the 7000 cm^{-1} region (Figure 10). The second portion of Table 1 also summaries our results and assignments. The details of our results and analyses are given in Appendix E.

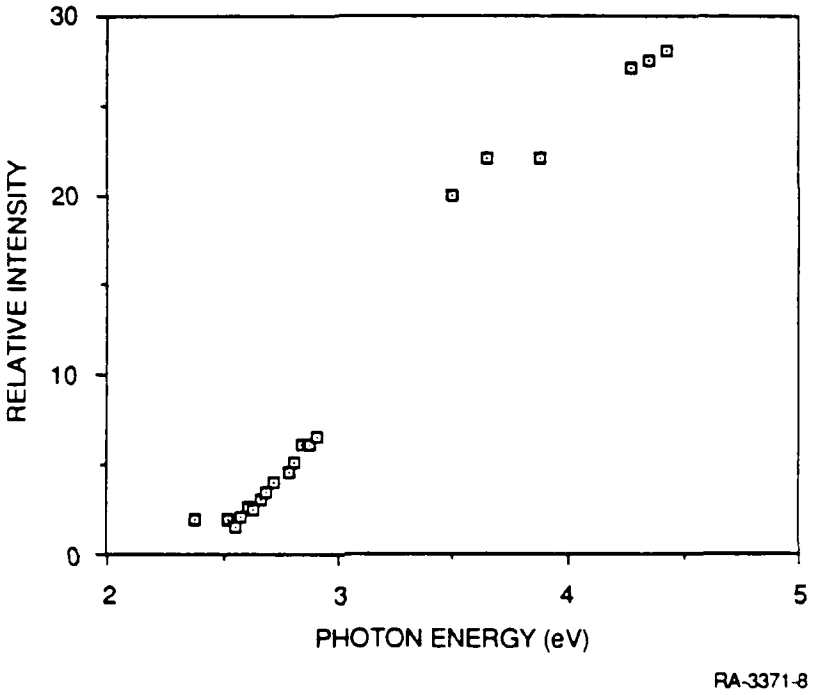

Figure 9. A photofragment spectrum of H_3^+ near the threshold of bound-free photodissociation into $H_2^+ + H$.

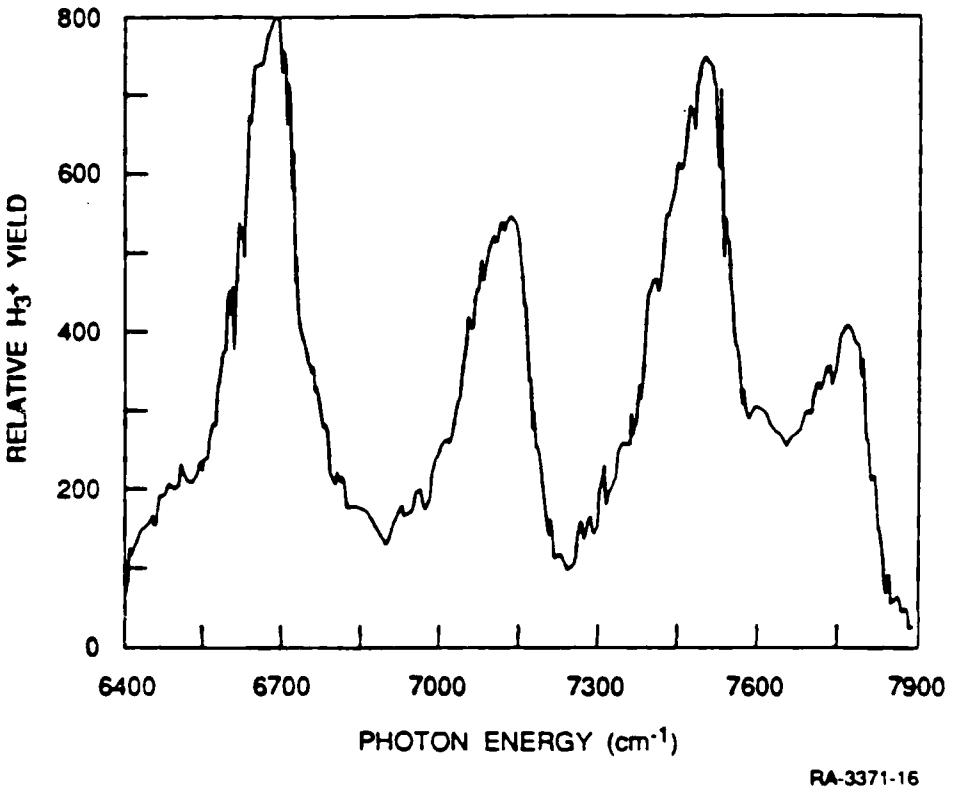

Figure 10. A photogragment spectrum of H_5^+.

Table 1

Photodissociation of H_5^+ and Vibrational Transitions

Okumura, Yeh and Lee Measurements

Observed Bands (cm^{-1})	Assignments
3532	ν_2
3910	ν_1
4230	$\nu_1 + \nu_8$ or $3\nu_4$

Bae Measurements

Observed Bands (cm^{-1})	Assignments
6690	$2\nu_2$
7130	$\nu_1 + \nu_2$
7490	$2\nu_1$
7770	$2\nu_1 + \nu_8$

Searches for Negative Hydrogen Cluster Ions

Although Bae et al.[17] ruled out the existence of triangular H_3^- and its isotopes, the existence of a stable linear form had remained uncertain. In their recent systematic, theoretical study of hydrogen negative cluster ions, Michels and Montgomery[18] predicted that the linear geometry of H_3^- is not stable but that D_3^- is bound by as much as 7 meV. They suggested that it may be possible to produce D_3^- by colliding D^- with a cold D_2 gas jet.

After modifying our source and searching for its optimum negative ion operating parameters, we successfully generated relatively intense beams of well known negative ion clusters such as $(CO_2)_n^-$. However, although we did not find H_3^- or its isotopes, we obtained the upper limits of the intensity ratios of H_3^- to H^- and D_3^- to D^- as 0.5% and 1.0%, respectively. A paper describing these results is in preparation.

CLUSTER-IMPACT FUSION

Almost at the end of this project, a new promising application of hydrogen-containing cluster ions for nuclear fusion was dicovered by Brookhaven scientests.[8] After discussions with the technical monitor we redirected towards investigation of the application of CIF as a fuel for rocket propulsion. Because CIF requires a very high intensity ion beam of large clusters containing deuterium, such as clusters of LiD, under the current contract, we have developed a new cluster ion source. The schematic diagram of the source is shown in Figure 11. The source is based on the combination of two key techniques: pulsed laser evaporation, and evaporation of materials in a subsonic inert gas in order to condense large clusters. We tested the source with carbon and successfully generated a very high flux of large (n > 1000) clusters.

Because LiD is very reactive and toxic, the new source was tested with carbon. The carbon vapor was evaporated from a rotating graphite rod by a focused beam of the second harmonic of a YAG laser in room temperature Ar gas. The laser energy density on the graphite was typically less than 2 J/cm^2 to prevent plasma generation. The Ar pressure was varied between 1-10 Torr. The evaporated carbon vapor condensed in the gas and formed large carbon clusters. The clusters were carried by the stream of Ar gas through a long (30 cm) 2 mm ID tube, ionized by electron impact, accelerated to 100 eV, mass selected by a 60° magnetic sector, and detected by a large Faraday cup. With the given setup the mass resolving power M/ΔM was only 2. Figure 12 shows the low mass end (size < 4000 atoms/clusters) of the size distribution of the generated carbon clusters. The relative current 100 in the figure corresponds to ~10^8 clusters/sec. The total integrated neutral flux measured before mass selection of all generated clusters was equivalent to 10^{18} carbon atoms/sec; the observed mass flux in the lower end, as shown in Figure 12, corresponds to only 10^{13}. Apparently the mean size of the clusters is much larger than 1000 atoms/cluster. A paper describing these results is in preparation.

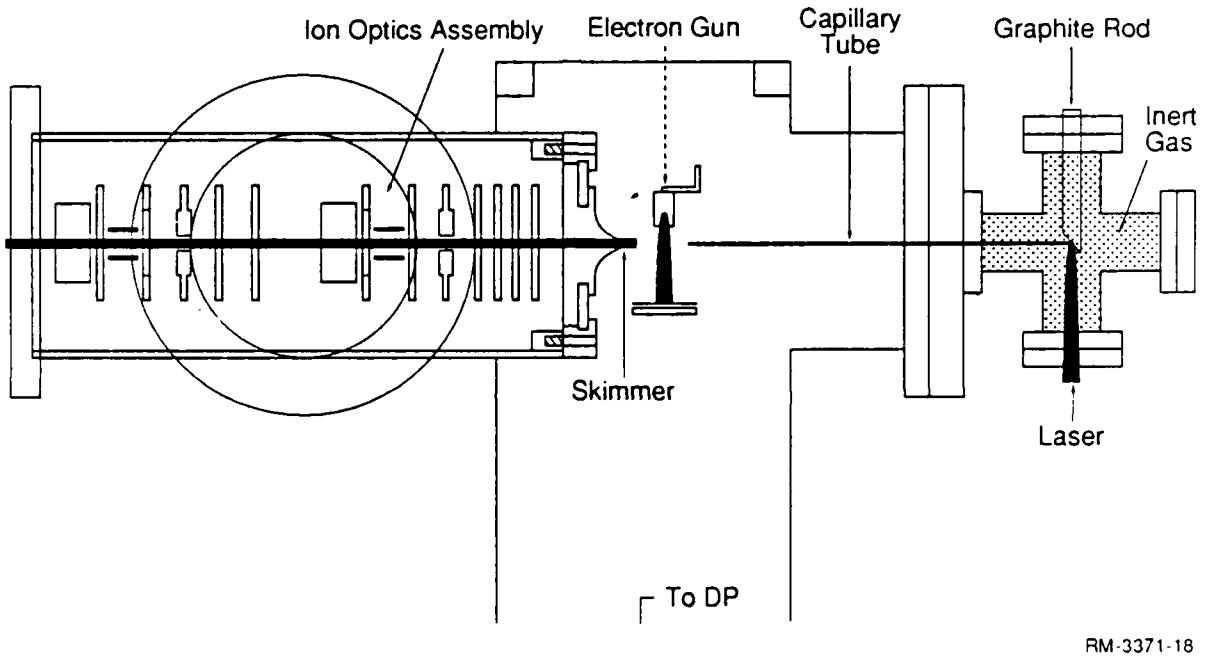

Figure 11. Schematic of the new high intensity cluster ion source.

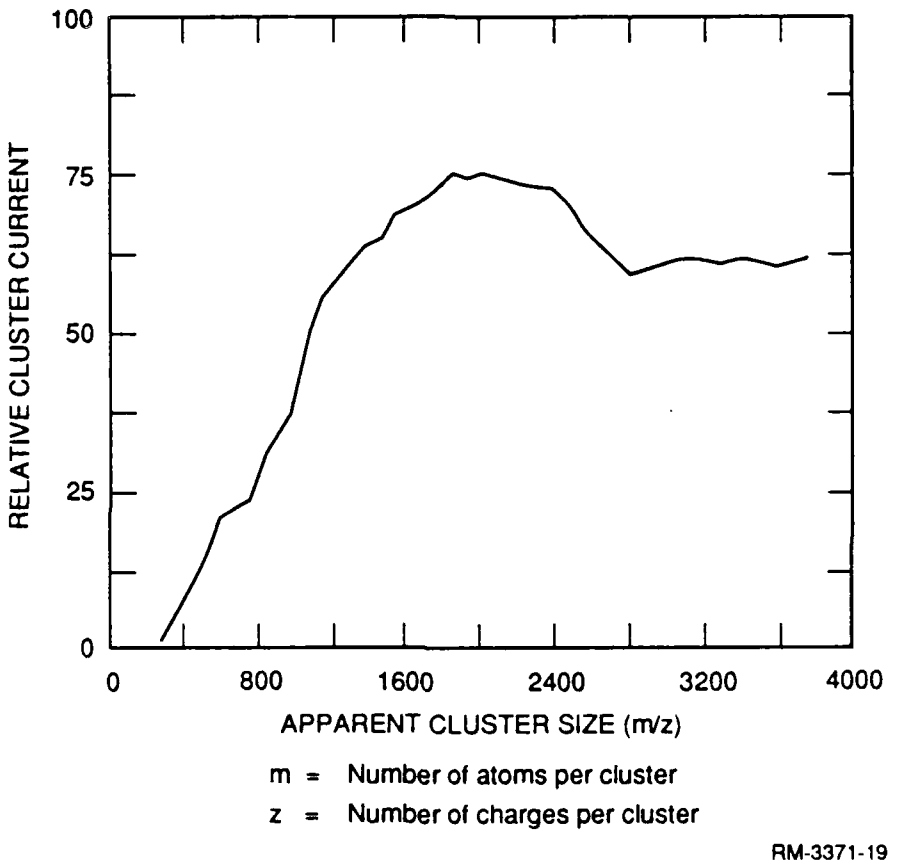

Figure 12. The low-mass end of the size distribution of generated carbon cluster ions.

CONCLUSIONS AND IMPLICATIONS FOR FUTURE WORK

We have demonstrated that the production of intense beams of positive hydrogen cluster ions is quite feasible, and should allow their rapid embedment in a H_2 matrix. However, stabilization of these species by codeposition of hydrogen cluster anions does not appear to be a useful approach, because of the extreme difficulty we have encountered in generating the negative hydrogen cluster beams. One approach which has not been investigated is to generate the stabilizing anion directly within the matrix. Whereas the hydrogen anion clusters may be unstable in the gas phase, within the matrix H^- may form a cavity by repelling the surrounding H_2 molecules to produce a locally stable structure. Anion generation within the H_2 matrix and explicit determination of the maximum storable densities and lifetimes of the positive ions within the matrix are subjects of future investigation.

A much more promising way of achieving an extremely high energy density for rocket propulsion is the use of hydrogen-containing cluster ions for igniting nuclear fusion (cluster-impact fusion, CIF). For instance, the energy density that can be achieved by CIF with the DT fuel is 3.4×10^{14} J/kg which is eight orders of magnitude larger than the energy density of LOX/H_2 (1.6×10^6 J/kg). For missions with $I_{sp}<10^5$ s, the CIF rocket performance will be essentially identical to that of antimatter. However, production and storage of CIF fuels will be straightforward, because it uses regular matter instead of antimatter.

Under the current project, we have developed new high intensity cluster ion sources which are essential for CIF experiments. Furthermore, we have added additional apparatuses, including a 300-kV electrostatic accelerator, to the existing cluster facility with the construction partly supported by the current project. In our next research, we propose to repeat Brookhaven results on the CIF experiment, then vigorously investigate various scientific and technological issues related to the feasibility of CIF for rocket propulsion. The new proposal entitled "Cluster Impact Fusion Propulsion" is submitted under a separate cover.

REFERENCES

1. Y. K. Bae, "Are the Geometrical Strucutres of H_{15}^+ and H_{27}^+ a Pentagonal Bipyramid and an Icosahedron?" submitted to Chem. Phys. Lett. (Appendix C)

2. K. Hirao and S. Yamabe, "Theoretical Study on the Structure and Stability of Hydrogen-Ion Clusters H_n^+ and H_n^- (n = 3,5,7,9,11,13)," Chem. Phys. Lett. **80**, 237 (1983).

3. A. van Lumig and J. Reuss, "Collisions of Hydrogen Cluster Ions with a Gas Target, at 200 - 850 eV Energy," Int. J. Mass Spec. Ion Phys. **11**, 483 (1978).

4. Y. K. Bae, in preparation.

5. T. Oka, private communication.

6. Y. K. Bae and P. C. Cosby, "Observation of Bound-Free Photodissociation of H_3^+," Phys. Rev. A**41**, 1741 (1990). (Appendix D)

7. Y. K. Bae, "Observation of High-Lying Vibrational Predissociation States of H_5^+," Submitted to Chem. Phys. Lett. (Appendix E)

8. R. J. Beuhler, G. Friedlander, and L. Friedman, "Cluster Impact Fusion," Phys. Rev. Lett. **63**,1292 (1989).

9. Y. K. Bae, in preparation.

10. Y. K. Bae, P. C. Cosby, and D. C. Lorents, "Observation of Shell Structures in the Growth of Microcluster Ions," Chem. Phys. Lett. **59**, 214 (1989).

11. Y. Yamaguchi, J. F. Gaw, and H. R. Schaefer, "Molecular Clustering about Positive Ion Structures, Energetics, and Vibrational Frequencies of the Protonated Hydrogen Clusters H_3^+, H_5^+, H_7^+, and H_9^+," J. Chem. Phys. **78**, 4047 (1983).

12. K. Hiraoka, "A Determination of the Stabilities of $H_3^+ (H_2)_n$ with n = 1-9 from Measurements of the Gas-Phase Ion Equilibria $H_3^+ (H_2)_{n-1} + H_2 = H_3^+ (H_2)_n$," J. Chem. Phys. **87**, 4048 (1987).

13. D. Talbi and R. Saxon, "Theoretical Study of Excited Singlet States of H_3^+: Potential Surfaces and Transition Moments," J. Chem. Phys. **89**, 2235 (1988).

14. B. Peart and K. T. Dolder, "The Production of De-Excited H_3^+ Ions and Measurements of the Energies of Two-Electronically-Excited States," J. Phys. B**7**, 1567 (1974).

15. Y. Yamaguchi, J. F. Gaw, R. B. Remington, and H. R. Schaefer, "The H_5^+ Potential Energy Surface: Characteristization of Ten Distinct Energetically Low-Lying Stationary Points," J. Chem. Phys. **86**, 5072 (1987).

16. M. Okumura, L. I. Yeh, and Y. T. Lee, "Infrared Spectroscopy of the Cluster Ions, $H_3^+ (H_2)_n$," J. Chem. Phys. **88**, 79 (1988).

17. Y. K. Bae, M. J. Coggiola, and J. R. Peterson, "A Search for H_2^-, H_3^-, and other Metastable Negative Ions," Phys. Rev. A**29**, 2888 (1984).

18. H. H. Michels and J. A. Montgomery, Jr., 'The Electronic Structure and Stability of the H_3^- Anion," Chem. Phys. Lett. **139**, 535 (1987).

APPENDIX A

A HIGH INTENSITY CLUSTER ION SOURCE FOR FAST BEAM EXPERIMENTS

A HIGH INTENSITY CLUSTER ION SOURCE FOR FAST BEAM EXPERIMENTS

Y. K. Bae, P. C. Cosby, M. Nicholson, and W. Olson

Molecular Physics Laboratory

SRI International

Menlo Park, CA 94025

ABSTRACT

A high intensity cluster ion source that can be used for various fast beam spectroscopic studies has been constructed and demonstrated. The cluster ions are grown around seed ions which are generated by electron impact ionization of gas very near the exit of the nozzle (~1 nozzle diameter distance). The generated cluster ions are coaxially focussed and extracted from the pulsed (10 Hz, 200 μsec pulse) supersonic expansion through a skimmer by applying a weak (~1 V/cm) electric field, and injected into a photofragment spectrometer. With the source we have successfully generated well-collimated intense beams of various positive and negative cluster ions, such as H_n^+, $H_3O^+(H_2)_n$, $(CO)_n^+$, $(N_2)_n^+$, $(CO_2)_n^+$, $(NO)_n^+$, He_n^+, Ne_n^+, Ar_n^+, Xe_n^+, and $(CO_2)_n^-$, with peak currents of ~500 pA at cluster size n = 10. Preliminary photofragmentation studies of selected cluster ions have been performed to demonstrate the capability of the source.

MP 90-128
July 31, 1990

I. INTRODUCTION

There has been considerable interest in recent years to understand the structure of small molecular clusters, since such species represent a tractable bridge between isolated molecules and the condenced phase. Charged clusters, referred to here as cluster ions, play a central role in these studies because mass spectroscopic techniques can be used to isolate clusters of a specific size. The price extracted for this advantage is that the density of the cluster ions is generally much less than that which can be achieved with neutral molecules. Despite the low density, a variety of techniques have been implimented to study the structure and dynamics of cluster ions.[1-3] Photofragment spectroscopy[4] of the cluster ions is proving to be useful in their study. Because the binding energy of clusters is quite small, absorption of even an infrared photon by the cluster ion generally provides sufficient energy to induce fragmentation. Thus the photoabsorption can be sensitively detected by observing the appearance of the charged cluster fragment. Energy or momentum analysis of this fragment provides additional insight by probing the dynamics of the fragmentation process.

Photofragment spectroscopy has been applied in a variety of cluster ion studies ranging from the infrared absorption spectrum of H_{2n+1}^+ (n = 1-7) clusters[5] to the visible and ultraviolet absorption properties and fragmentation dynamics of Ar_n^+ (n = 3-40) clusters.[6] Essentially any cluster ion can in principal be generated, but not always in sufficient concentration to allow its useful investigation.

We report here a cluster ion source that is useful for generating well-collimated, intense beams of various homogeneous or mixed species of positively or negatively charged cluster ions. The ion source is relatively simple to construct and also very stable. Several photofragment studies on various small cluster ions have been performed with the source and a pulsed YAG laser system

in our newly built cluster facility. It seems that the applications of the source for photofragment studies of various larger cluster ions are relatively straightforward.

II. ION SOURCE

The present cluster ion source produces high intensity cluster ion beams by generating abundant seed ions which nucleate the condensation of neutrals for the growth of the cluster ion within a pulsed, supersonic expansion of gas. These seed ions are produced early in the expansion by electron impact ionization of the gas very near the exit of a supersonic nozzle:

$$X + e \rightarrow X^+ + 2e. \qquad (1)$$

For the specific case of an H_2 expansion, the nascent ion produced by electron impact is H_2^+, but this quickly reacts to form H_3^+, which serves as the core ion for further cluster growth. In most other systems, however, no rapid two-body reaction channel is accessible to the positive ion produced in (1), and X^+ serves directly as the initial seed ion to nucleate the cluster growth.

Growth of the cluster ion occurs in a series of three-body association reactions:

$$X^+ \cdot X_n + X + M \rightarrow X^+ \cdot X_{n+1} + M \quad (n = 0,1,...) \qquad (3)$$

where the product ion of the association reaction serves as the core for the subsequent association. The ion-molecule association reactions are dominated by two very strong interactions, charge delocalizaiton and ion-neutral polarization, which are in general much stronger than the van der Waals interaction that controls cluster growth in a neutral system. For example, the association energy of H_3^+ and H_2 is ~2000 cm^{-1}, whereas that of H_2 and H_2 is only a few cm^{-1}. This large disparity in the interactions allows expansion conditions to be chosen in which substantial cluster

ions can be grown in the absence of neutral clusters. Associative growth of the cluster ion has the particular advantage in that excess heat of the reaction can be dissipated as translational or internal energy in the third body M. In contrast, when the cluster ion is produced by direct ionization of a neutral cluster, the excess heat is primarily dissipated by fragmentation. The key element in a satisfactory cluster ion source design is to produce the seed ion very early in the gas expansion, which typically retains adequate densities for rapid three-body association reactions over a free expansion distance ot about 10 nozzle diameters.

The cross sectional drawing of the the ion source assembly, together with its vacuum envelope, skimmer, and associated optics for the acceleration and collimation of the cluster ions is shown in Figure 1. The various elements are placed roughly to scale. The diffusion pump indicated in the figure is a 10 inch model backed by a 60 cfm mechanical pump. The source assembly is mounted on a manipulation port which allows tilt adjustments on two axes orthogonal to the ion beam plus translation of the assembly along the ion beam direction. The purpose of these adjustments is to allow precise positioning of the assembly relative to the skimmer and ion optics, which are fixed to the apparatus. The pulsed supersonic jet was obtained by expanding 1-5 atm gas at room temperature through a 1-mm-ID and 2-cm-long stainless steel capillary tube. The tube is essential for localizing the ionizing electron beam very close to the exit of the nozzle. The tube was welded to the outlet port of a commercial piezoelectrically-activated pulsed valve (Lasertechnics) operated at 10 Hz with the pulse duration of 200 μs. When the pulsed valve was operating at this rate, the time averaged pressure in the source vacuum chamber rose from 1×10^{-6} to 2×10^{-5} Torr.

The electron beam was generated continously from a filament of 10 mil tungsten wire bent in a "U" shaped configuration with a 5-mm flat active area by passing a current of typically 10A through the filament wire. Electrons emitted by the wire were accelerated to 200 eV through 90 % transparent grid positioned 1 mm away from the filament. The grid formed one end of an 8mm diameter stainless steel cylinder that enclosed the electron gun assembly. Various positions of the

electron gun assembly were tested for the generation of cluster ions. The optimum position found for the electron gun assembly placed the grid a radial distance of 6 mm from the exit of the capillary tube, with the axis of the gun a distance of 1 mm from the capillary tube exit. Electrons leaving the gun assembly and escaping collection by the nozzle impinge on a flat stainless steel collection plate located 25 mm radially opposite to the gun assembly. The electron gun assembly, the gas capillary tube, and the electron collection plate were maintained at the same electrical potential (V_S) to minimize stray fields in the ionization region. The potential V_S = 2-10 kV establishes the final kinetic energy (E_0 = 2-10 keV)of the cluster ions, following their acceleration to ground potential in the region beyond the skimmer. Under typical source operating conditions, an electron current of 2 mA is measured on the collection plate.

Gas flow in the ionization region is controlled by the Lasertechnics pulsed value driven by an electrical pulse of ~180 V. The generator providing this pulse was constructed based on the circuit provided by the manufacturer, modified by the addition of an optoisolater (TRW OPI120) to provide electrical isolation of the trigger input signal from V_S. When initially installed in the apparatus, the operating characteristics of the valve were found to continuously drift with time such that the valve ceased opening after several hours of operation. This was found to be caused by a heating of the value by the electron gun assembly and was corrected by providing water cooling to the valve body. With this water cooling the source became much more stable and could be continuously operated for several days without any major adjustment. This stability was essential to the laser photofragment studies, because a single scan often lasts more than several hours.

III. ION BEAM FORMATION AND ACCELERATION

A conical skimmer with a 2 mm ID entrance aperature is located 5 cm away from the exit of the nozzle, as shown in Fig. 1. Ions created near the nozzle are gently accelerated and focused by a weak potential difference (1-4 V/cm) applied between the skimmer and the nozzle. After passing the skimmer the ions were progressively accelerated through a series of three 3 mm aperatures to

ground potential and focussed by a symmetric einzel lens (EL1) through a 3mm image aperature. Ions passing through this aperature are collimated to a parallel beam by a second symmetric einzel lens (EL2). Both lenses were operated at an electrical potential on their central elements equal to roughly 2/3 of the ion beam energy. Vertical and horizontal deflection plates follow each einzel lens to allow small corrections to the ion beam direction. Voltages applied to the deflection plates were usually less than 1/10 of the beam accleration voltage. The skimmer and the ion optics are installed in a separate vacuum chamber pumped by a 6 inch diffusion pump. With the source in operation, the time averaged pressure in this chamber rose from 4×10^{-7} to 2×10^{-6} Torr.

The accelerated and collimated cluster ion beam is mass selected by a 40 cm radius, 60° electromagnetic sector which is capable of bending 5500 keV-amu ions, and passes through a 3mm diameter aperature into a 90 cm long field-free interaction region, as illustrated in Figure 2. This 3mm aperature yields an effective mass resolution $\Delta M/M = 0.019$ for a 2000 eV ion beam. The field free interaction region is terminated by a Faraday cup with a 10 mm diameter entrance aperature. Electrostatic deflection plates at the entrance to the field free interaction region allow the ion beam to be directed through a 3mm diameter hole at the center of the Faraday cup and into an 127 cylindrical electrostatic energy analyzer. This analyzer, with a mean radius of 5.5 cm, allows dispersion of the ion beam kinetic energy with a resolution of 3%. Ions passing through the energy analyzer are detected by a microchannel plate electron multiplier. Vacuum chambers enclosing the magnet/interaction region and the Faraday cup/electrostatic analyzer/detector are each pumped by 6-inch diffusion pumps, with base pressures in these regions of 2×10^{-7} Torr, that are largely independent of source gas load. As indicated in Fig. 2, optical windows are provided in both the magnetic sector and the detector chambers, which together with 3mm diameter clearance holes in the electrostatic sector and in the Faraday cup, allow colinear overlap of a laser beam with the ion beam over the length of the interaction region.

IV. FRAGMENT GENERATION AND DETECTION

Dissociation of a molecular ion of mass M in the interaction region into fragments produces an equipartitioning of the molecular ions's momentum among those of its fragments. For the case where only two fragments are produced with masses M_A and M_B from the molecular ion of mass $M = M_A + M_B$ and kinetic energy E_0, the (laboratory) kinetic energy of the charged fragment (designated A) will be:

$$E_A = \frac{M_A E_0}{M}(2\cos^2\theta - 1) + \frac{M_B W}{M} \pm \frac{2M_A M_B \cos\theta}{M}\left(\frac{E_0 W}{M_A M_B} - \frac{E_0^2 \sin^2\theta}{M_B^2}\right)^{1/2} \qquad (4)$$

where Θ is the laboratory angle with respect to the molecular ion direction at which the fragment is detected and W is the internal energy of the molecular ion, in exesss of that required for dissociation, that is partitioned to translational energy of its fragments. The angle Θ lies in the range $0 \le \Theta \le \Theta_{max}$, where

$$\Theta_{max} = (M_B W/M_A E_0)^{1/2}. \qquad (5)$$

In the dissociation of a typical singly-charged cluster ion, one or more of its fragments is typically a polyatomic species (ion or neutral) with a large number of internal degrees of freedom. Hence the excess energy that will be partitioned into translational energy will be typically quite small ($0 \le W \le 0.01$ eV).[7] In this limit of $W \rightarrow 0$, equation (4) reduces to

$$E_A = M_A E_0/M, \qquad (6)$$

which is valid regardless of the number of fragments produced in the dissociation or of whether they are produced simultaneously or sequentially. Since E_0 is established by the acceleration from

the ion source potential, the energy dispersion of the electrostatic analyzer affords a mass spectrum of the charged fragments produced by dissociation of the cluster ion of mass M.

Charged particles that pass through the electrostatic analyzer impinge on a pair of microchannel plates for detection. These plates are operated in one of two modes chosen with respect to signal intensity. For strong signals, such as encountered with the primary ion beam, the front surface of the first MCP is directly connected to an electrometer, with the plate serving as a Faraday cup. For low level signals, however, a potential difference of ~1000 V is applied across each MCP, such that the secondary electrons produced by an ion striking the first plate produces an amplified cloud (~10^7) of electrons that is collected on an impedance-matched anode following the MCP pair. The charge of the electron cloud is converted into a TTL pulse by an external preamplifier and pulse amplifier/discriminator and is detected by a pulse counter (BiRa Model 2101).

The minimum fragment flux detectable in the pulse counting mode is set by the dark count rate of the MCP plates (~200 s^{-1}). By gating the counter in coincidence with the ~200 μs primary ion beam pulse, the minimum fragment flux is reduced to 0.04 per ion source pulse. A much narrower gate width may be used for the collection of photofragments produced by a pulsed laser. Because the laser pulse width (10 ns) is very narrow in comparison to the time required for a cluster ion to traverse the 60 cm laser interaction region (7μs), only those cluster ions present in that region at the time of the laser pulse will be irradiated and can produce photofragments. These photofragments, after a time delay, must arrive at the MCP detector within this same 7μs period. By gating the counter in coincidence with the arrival of photofragments, the effective dark count rate is reduced to 0.0014 per laser shot. At this level, the MCP dark counts are negligible and the minimum detectable signal is determined by the rate of background dissociation of the parent ions (spontaneous dissociation and/or collision-induced dissociation) within the laser interaction region. These background fragments are accumulated by gating open a second channel of the counter for an equal period of time following the arrival of all photofragments produced by a laser pulse. The

photofragment signal is obtained from the difference of the laser on and laser off counter registers following a fixed number of laser shots (typically 100). The maximum detectable fragment flux in the pulse counting mode is set by the pulse pair resolution of the counter and the Poisson statistics[8] of the fragmentation at 30 per laser shot.

A series of delay generators controls the firing of the pulsed laser and the gating of the two counter channels, in synchronization with the opening of the pulsed valve in the ion source. The contents of the counter registers are recorded in an IBM PC/AT compatible microcomputer via a CAMAC crate controller. The microcomputer also controlled and monitored the electromagnet, electrostatic analyzer, and dye laser wavelength.

V. RESULTS AND DISCUSSION

Well collimated high intensity beams of various cluster ions, such as H_n^+, $H_3O^+(H_2)_n$, $(CO)_n^+$, $(N_2)_n^+$, $(CO_2)_n^+$, Ar_n^+, Xe_n^+, $(NO)_n^+$, He_n^+, Ne_n^+, and $(CO_2)_n^-$ have been generated. The ion current dependence on cluster size has been discussed previously,[9] in particular for the first seven of these species.

As indicated by the formation $H_3O^+(H_2)_n$ in the expansion of (nominal) H_2 gas, mixed species cluster ions can be produced with the ion source by mixing the composition of the expanding gas. Figure 3 shows the mass distribution of ions, observed at the Faraday cup, that are produced from a 8:2 mixture of N_2 and O_2 in the ion source expansion gas. Between the main series of $(N_2)_n^+$ cluster ions, four additional series of cluster ions were observed. These series correspond to $[(N_2)_{n-1}\bullet O_2]^+$, $[(N_2)_{n-2}\bullet(O_2)_2]^+$, N_{2n+1}, and $[(N_2)_n\bullet H_2O]^+$ respectively. The series containing H_2O resulted from a small impurity of water in the gas.

We have also generated negative ion clusters. As an example, Figure 4 shows the mass distribution of negative ions produced from a CO_2 expansion. The ion source operating parameters for generating the negative cluster ions are quite different from those for positve cluster ions. The negative cluster ion currents maximized at electron beam energies less than 10 eV

(instead of 200 eV) and a very large skimmer potential, -100 V relative to the pulsed valve (instead of -10 V), was required to observe these species. DeLuca et al.[10] have postulated that the negative cluster ions are formed by the dissociative attachment to neutral clusters of slow electrons, cooled by inelastic collisions within the jet. This is consistent with the absence of the CO_2^- monomer ion from the mass spectrum shown in Fig. 4, and by the absence of CO_3^-.

To demonstrate the capabilities of the cluster ion source, we have measured the photofragment spectra of several species. The results from two of these species, bound-free photodissociation[11] of H_3^+ and the ir photoabsorption/photofragmentation[12] of H_5^+, have been presented elsewhere. We will briefly discuss here the results of photofragmentation studies of low order $(CO)_n^+$ clusters, which have especial importance because photodissociation of the dimer ion has been previously studied by another technique.

Figure 5 shows the wavelength dependence of the production of CO^+ from $(CO)_2^+$ (solid curve) and the production of $(CO)_2^+$ from $(CO)_3^+$ (dashed curve) observed as the frequency doubled output from YAG-pumped dye laser was tuned between 278 nm and 288 nm. The photoabsorptions in each of these species are extremely strong. For 1 mJ laser pulse energies, the primary ion beam current had to be reduced more than two orders of magnitude below its optimum value to maintain the photofragment count rate within the maximum (30/shot) required for pulse counting. Oscillations in the production of CO^+ from $(CO)_2^+$ have been observed as a function of wavelength by Ostrander, Sanders and Weisshaar[13] in a fast flow reactor and attributed to vibronic structure in the (predissociated) excited state of the dimer ion. As shown in Fig. 5, we observe similar oscillations in not only the dimer ion, but also the trimer, suggesting that the trimer consists of a CO adduct attached to a dimer ion core: $(CO)_2^+ \bullet CO$.

We have also measured partial photodissociation cross sections for $(CO)_n^+$ cluster ions up to n = 5 at two wavelengths, 532 and 355 nm, by using the second and third harmonics of a YAG laser. The results are summarized in Table 1. It should be noted that the photodissociation cross section of $(CO)_2^+$ is quite small at these two wavelengths, less than 10^{-19} cm^2, in agreement with

the upper limits reported by Smith and Lee[14] in their drift tube photodestruction measurements and with the apparent photodissociation threshold near 313 nm observed by Ostrander, et al.[13] It is very interesting to note that the $(CO)^+$ fragment channel are very weak for the clusters larger than the $(CO)_2^+$ at 532 nm. At 355 nm the channel is very strong for $(CO)_3^+$, but becomes very weak for the clusters larger than $(CO)_3^+$. At both wavelengths the total photodissociation cross sections become gradually smaller as the cluster becomes larger. Extension of this study to the wider wavelength region and larger $(CO)_n^+$ cluster ions will be very exciting.

ACKNOWLEDGEMENT

This research was supported by the Indenpendent Research and Development Program of SRI International and by the Air Force Astronautics Laboratory (Contract F04611-87-C-0025). We gratefully acknowledge the technical contributions of S. Young to building electronics for the apparatus.

REFERENCES

1. T. D. Mark and A. W. Castleman Jr. in *Advances in Atomics and Molecular Physics*, D. Bates and B. Bederson, Eds. (Academic, Orlando, 1984) V. **20**, p. 65.

2. T. A. Miller and V. E. Bondeybey in *Molecular Ions: Spectroscopy, Structure, and Chemistry* (North-Holland, Amsterdam, 1983).

3. R. J. Saykally and C. S. Gudeman, Ann. Rev. Phys. Chem. **35**, 387 (1984).

4. J. T. Moseley in *Advances in Chemical Physics*, **60**, 245 (1985).

5. M. Okumura, L. I. Yeh, and Y. T. Lee, J. Chem. Phys. **88**, 79 (1988).

6. N. E. Levenger, D. Ray, M. L. Alexander, and W. C. Lineberger, J. Chem. Phys. **89**, 5854 (1988).

7. This need not always be the case. See M. F. Jarrold, A. J. Illies, and M. T. Bowers, J. Chem. Phys. **81**, 222 (1984).

8. R. L. Klobuchar, J. J. Ahumada, J. V. Michad, and P. J. Karol, Rev. Sci. Instrum. **45**, 1073 (1974).

9. Y. K. Bae, P. C. Cosby, and D. C. Lorents, Chem. Phys. Lett. **159**, 214 (1989).

10. M. J. DeLuca, B. Niu, and M. A. Johnson, J. Chem. Phys. **88**, 5857 (1988).

11. Y. K. Bae and P. C. Cosby, Phys. Rev. A **41**, 1741 (1990).

12. Y. K. Bae, Submitted to Chem. Phys. Lett.

FIGURE CAPTIONS

Figure 1. Cross sectional view of the ion source assembly (to scale). Also shown is the skimmer and ion beam acceleration and collimation optics.

Figure 2. Cross sectional view of the fast cluster ion beam apparatus. Vacuum pumps are not shown.

Figure 3. Mass spectrum of positive cluster ions generated with a N_2 and O_2 gas mixture. The current of $(N_2)_{10}^+$ measured at the faraday cup is 500 pA.

Figure 4. Mass spectrum of negative cluster ions generated with a CO_2 expansion. The current of $(CO_2)_3^-$ measured at the faraday cup is 10 pA.

Figure 5. Relative photofragment cross sections as a function of laser wavelength: CO^+ from $(CO)_2^+$ (solid curve); $(CO)_2^+$ from $(CO)_3^+$ (dashed curve).

TABLE 1

Partial photofragment cross sections of $(CO)_n^+$ cluster ions

Primary Ion	Fragment	Cross Sections in $10^{-22}cm^2$ 532 nm	355 nm
$(CO)_2^+$	$(CO)^+$	140	70
$(CO)_3^+$	$(CO)^+$	6	320
	$(CO)_2^+$	90	220
$(CO)_4^+$	$(CO)^+$	3.1	10
	$(CO)_2^+$	40	40
	$(CO)_3^+$	3.0	3 1
$(CO)_5^+$	$(CO)^+$	1.2	1.5
	$(CO)_2^+$	25	18
	$(CO)_3^+$	0.6	1.4
	$(CO)_4^+$	0	0

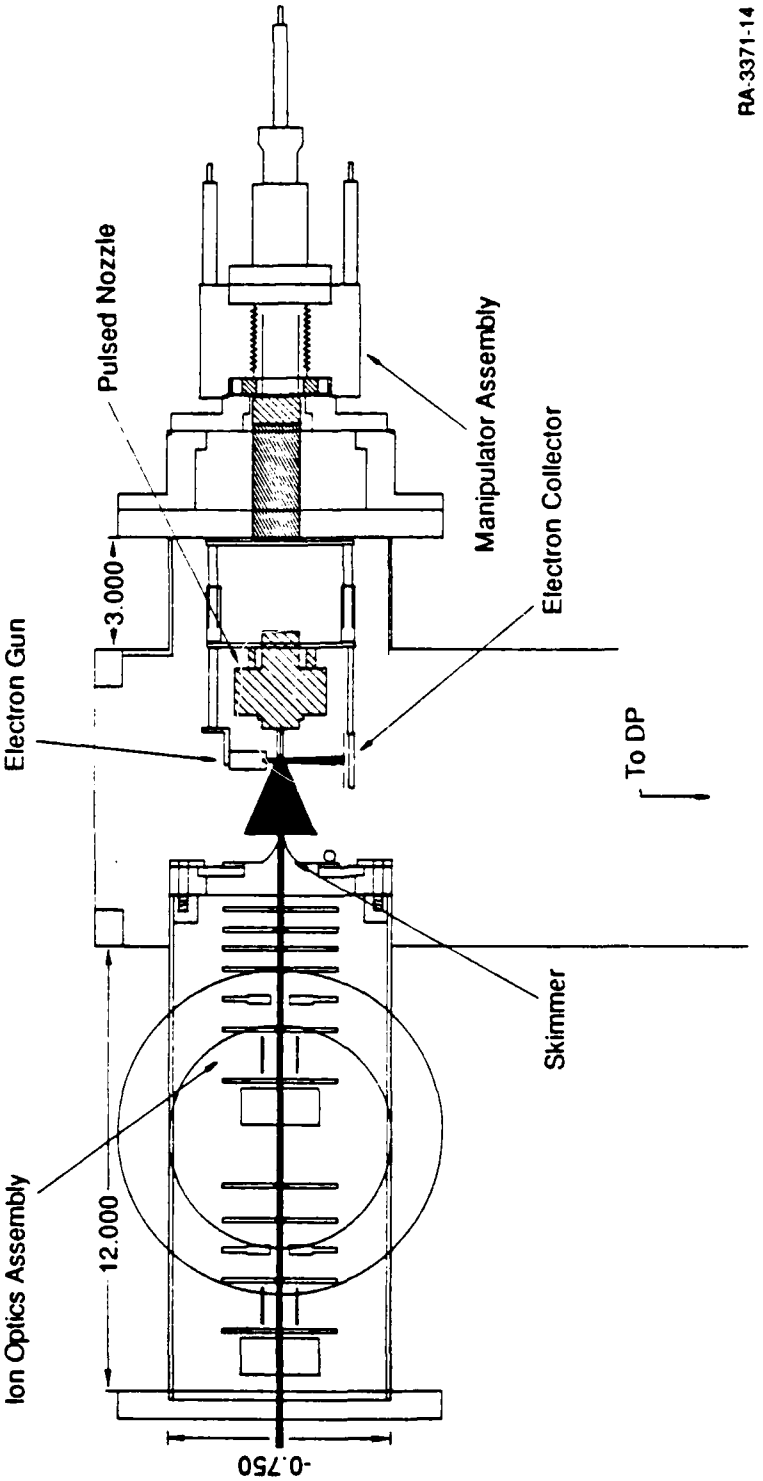
RA-3371-14
Pulsed Nozzle
Manipulator Assembly
3.000
Electron Collector
Electron Gun
To DP
Skimmer
Ion Optics Assembly
12.000
0.750

Figure 1

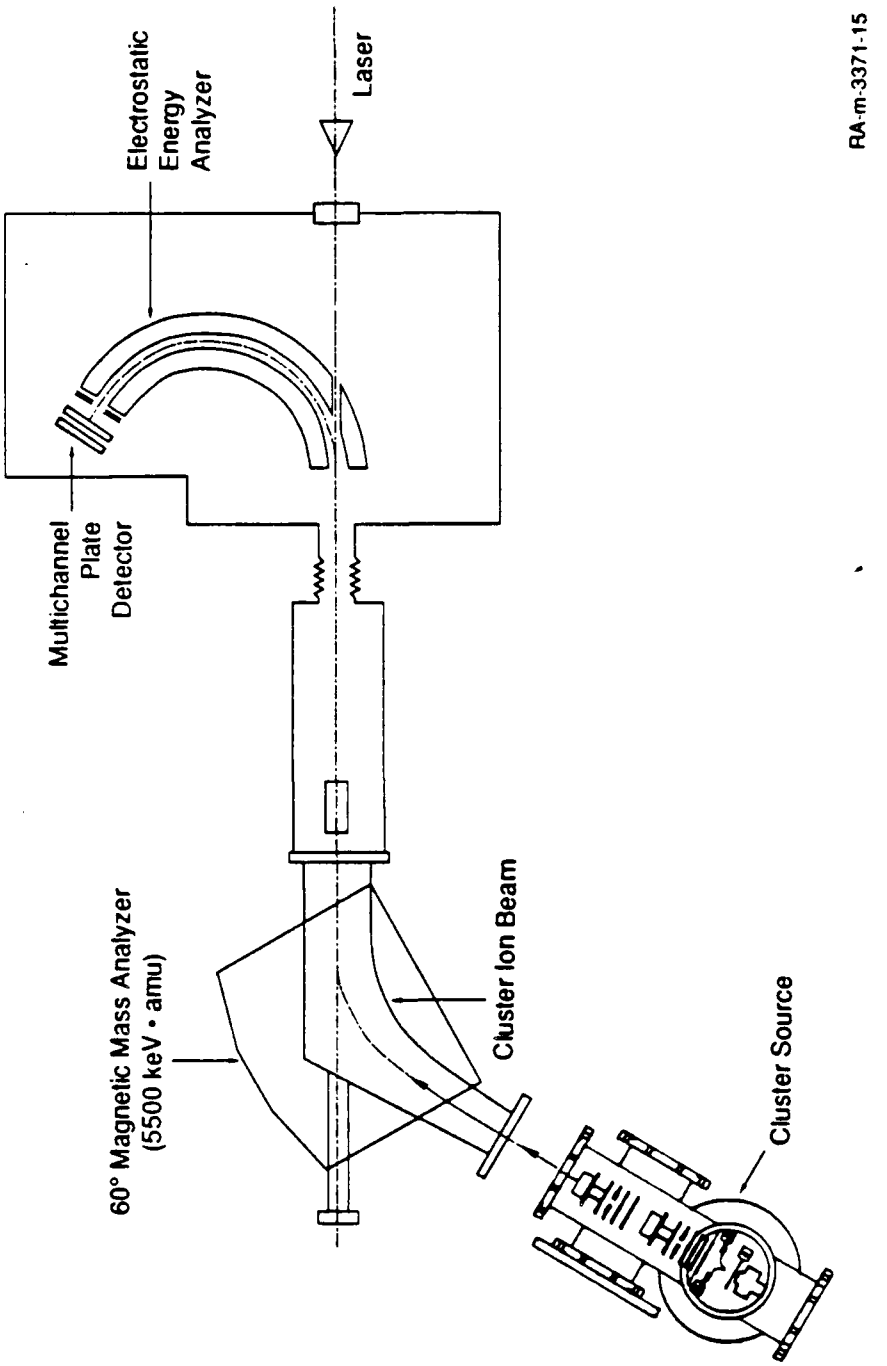
Electrostatic
Energy
Analyzer
Laser
Multichannel
Plate
Detector
60° Magnetic Mass Analyzer
(5500 keV • amu)
Cluster Ion Beam
Cluster Source
RA-m-3371-15

Figure 2

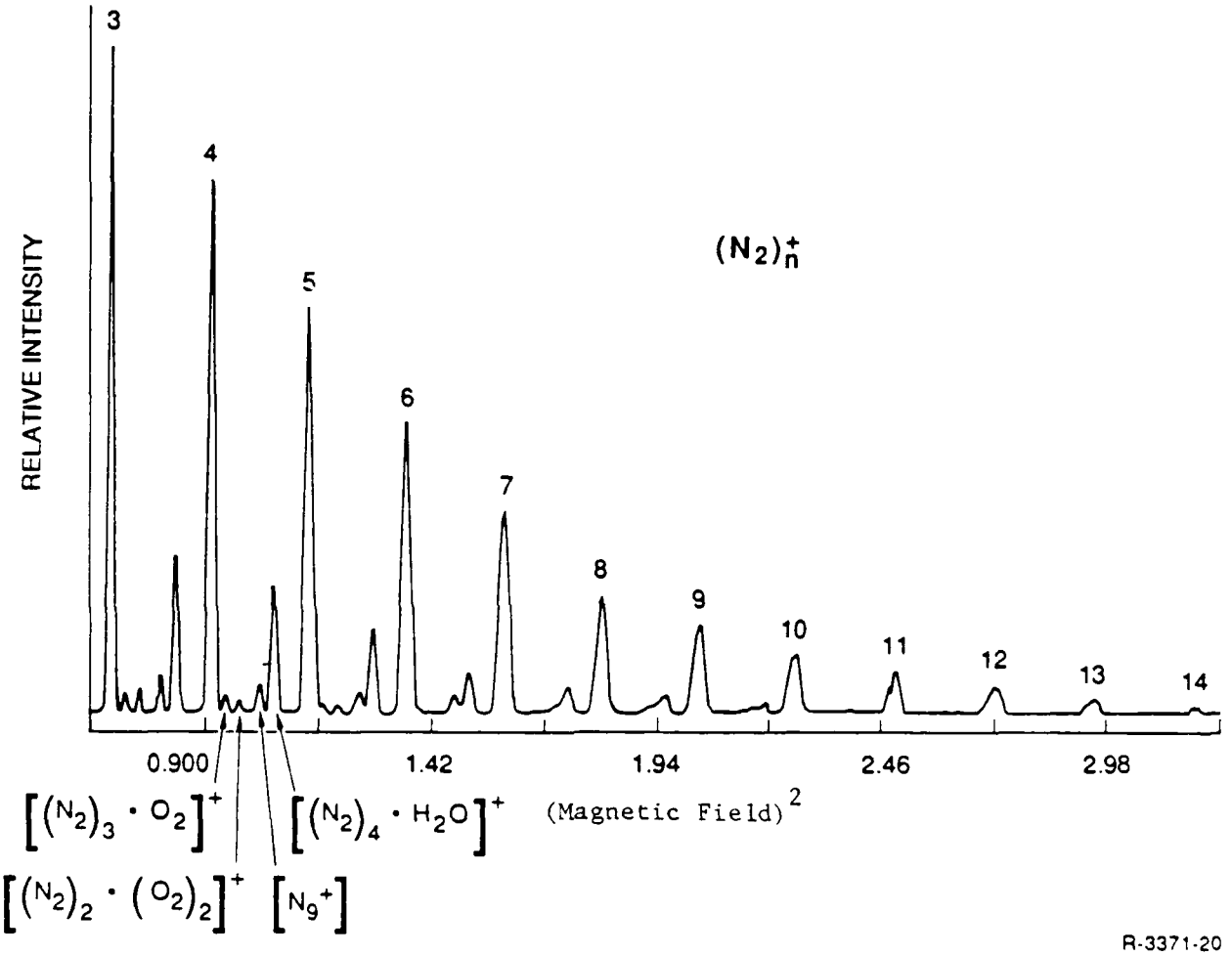
3
4
5
6
7
8
9
10
11
12
13
14
$(N_2)_n^+$
RELATIVE INTENSITY
0.900
1.42
1.94
2.46
2.98
$[(N_2)_3 \cdot O_2]^+$
$[(N_2)_4 \cdot H_2O]^+$
(Magnetic Field)^2
$[(N_2)_2 \cdot (O_2)_2]^+$
$[N_9^+]$
R-3371-20

Figure 3

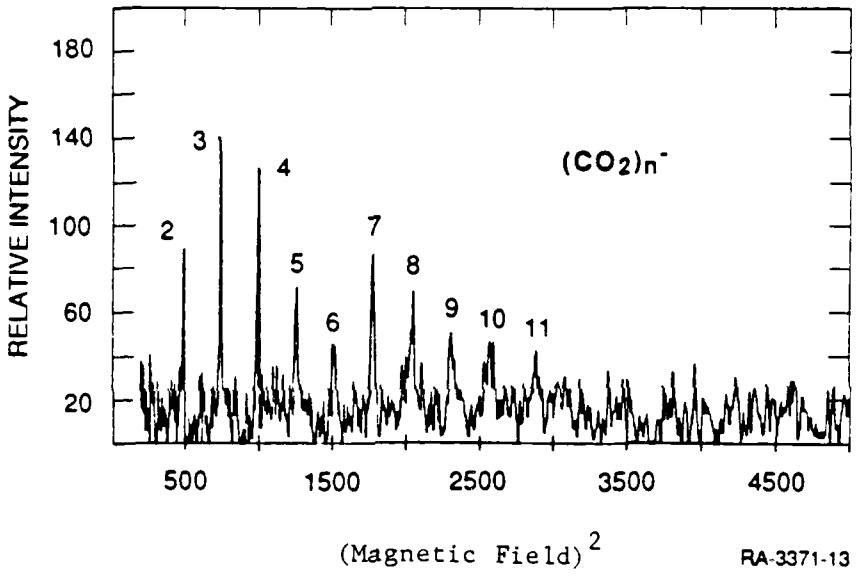
RELATIVE INTENSITY
180
140
100
60
20
2
3
4
5
6
7
8
9
10
11
$(CO_2)n^-$
500
1500
2500
3500
4500
(Magnetic Field)^2
RA-3371-13

Figure 4

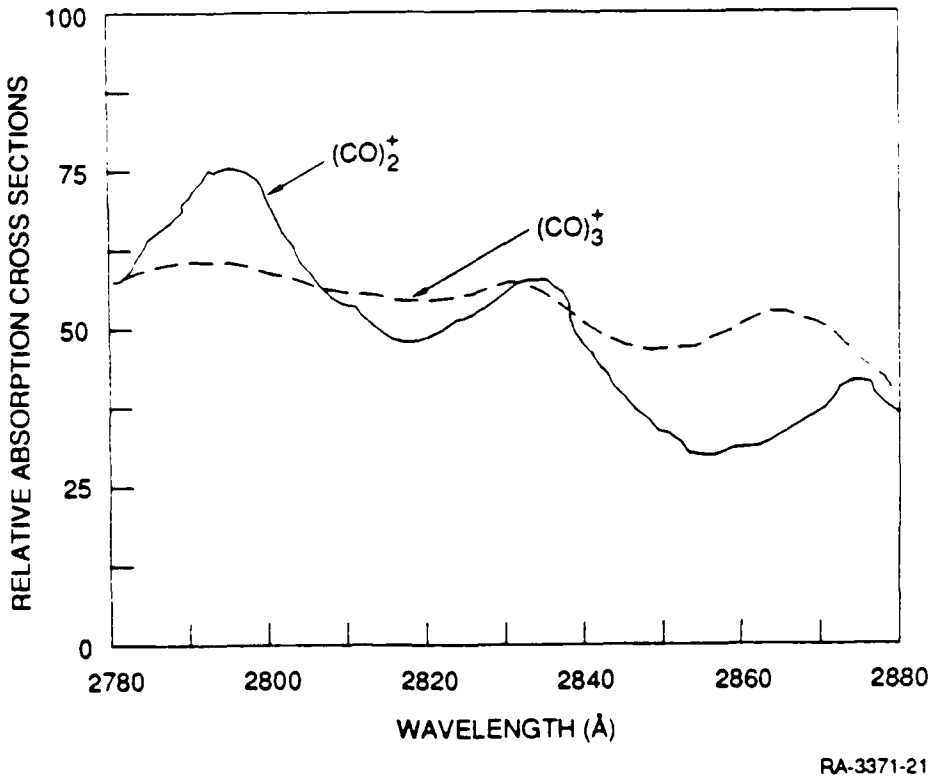
100
75
50
25
0
RELATIVE ABSORPTION CROSS SECTIONS
$(CO)_2^+$
$(CO)_3^+$
2780
2800
2820
2840
2860
2880
WAVELENGTH (Å)
RA-3371-21

Figure 5

APPENDIX B

OBSERVATION OF SHELL STRUCTURES IN THE GROWTH OF MICROCLUSTER IONS

REPRINTED WITH PERMISSION

OBSERVATION OF SHELL STRUCTURES IN THE GROWTH OF MICROCLUSTER IONS

Y.K. BAE, P.C. COSBY and D.C. LORENTS
Molecular Physics Laboratory, SRI International, Menlo Park, CA 94025, USA

Received 22 March 1989; in final form 1 May 1989

We have observed shell structure manifested in the size distributions of various non-metallic cluster ions sequentially grown on seed positive ions generated by electron impact ionization in a pulsed supersonic jet. The data suggest the identification of the core ion and the placement of equivalent ligands about the core during the embryonic stages of cluster growth. A crown structure similar to that of $H_3^+(H_2)_n$ is indicated for $H_3O^+(H_2)_n$ ($n \leq 4$). Pentagonal bipyramid structures with five neutrals surrounding a dimer ion core are suggested by the $(CO)_n^+$ ($n \leq 19$) and $(N_2)_n^+$ ($n \leq 14$) cluster size distributions, whereas $(CO_2)_n^+$ ($n \leq 16$) clusters appear to have a relatively amorphous structure. Variations in the cluster size distributions of Xe_n^+ ($n \leq 26$) are correlated with the elongated icosahedral structure.

1. Introduction

The question of how clusters grow in their embryonic stage has been of strong research interest for many years [1,2]. Although the growth of neutral van der Waals clusters is theoretically described in terms of a fivefold symmetric hard-sphere packing model [3,4], its experimental verification has encountered a difficult problem: without ionizing the clusters, i.e. without significantly disturbing them, they are generally not observable. The effect of this disturbance has been found to be much stronger in weakly bound van der Waals clusters than in strongly bound metal and semiconductor clusters [2]. Recent photofragment studies of the charged analogs of van der Waals clusters [5–7] have indicated that the magic numbers observed in cluster ion distributions represent the stability of the ions rather than that of the neutral precursor [8]. Accumulating evidence further indicates that the seed or embryo for the ionized cluster is not a monomer, as expected for a neutral cluster, but ionic dimers, trimers, or tetramers. Thus, cluster ions may have quite different structures from their neutral analogs [5–10].

The difference between the cores expected in the neutral and in the ionic clusters is a consequence of bonding forces. Van der Waals bonding exists in both the neutral and the ionized cluster. However, two stronger interactions dominate in the ionized cluster: hole delocalization and ion–neutral polarization. It is predicted [9,10] that the structure of small ionic clusters is mainly determined by competition between these two strong interactions. In rare-gas cluster ions, the well-defined p characteristics encourage hole delocalization by an initial linear growth of the ionic core [9,10], whereas the more diffuse charge distribution of molecular ions suggests that polarization forces will play a greater role in the early stages of cluster growth. For example, small molecular cluster ions, such as $(CO)_n^+$ [11,12] and $(CO)_n^+$ [13] have been either predicted or observed to have dimer ion cores, whereas Ar_n^+ [6,7,9,10] and Xe_n^+ [9,10] clusters have trimer ion cores.

In this paper, we report observation of shell structures in the very early stages of growth of various nonmetallic cluster ions. The intensity of the cluster ions, observed as a function of size (mass), is found to exhibit a strong regularity which reflects the growth of ligand shells around a core ion of particular structure.

2. Experimental

A detailed description of the apparatus used in this research will be given elsewhere [14]; only a brief

0 009-2614/89/$ 03.50

description is given here. Cluster ions were grown by clustering neutrals around seed ions, which have been generated by electron impact ionization in the early stage of a free supersonic expansion [5–7]. The supersonic jet was obtained by expanding 1 atm of the pure, room-temperature gas from a pulsed, water-cooled piezoelectric valve through a 1 mm inner diameter, 2 cm long tube. The valve was operated at 10 Hz with a pulse duration of approximately 200 μs. The continuous electron beam was generated from a single loop of 10 mil tungsten wire located 2 cm radially and 1 mm axially from the exit of the tube. Electrons produced by the filament were accelerated through a fine mesh electrode to 200 eV and directed near the exit orifice of the tube. The current of electrons collected after passing the tube was typically 2 mA. Neutral clustering is not extensive under these source conditions [5–7]. Cluster ions were formed mainly from nucleating about seed ions via three-body association reactions.

The generated cluster ions are gently focused by a potential applied to a skimmer (1 V/cm), pass through the skimmer positioned at a distance 3 cm from the tube, accelerated to 1.0 or 1.5 keV, and collimated by sets of ion optics. The cluster ions are then mass selected by a 60° magnetic sector, pass through a 90 cm long field-free region and a 127° electrostatic energy analyzer, and impinge on a microchannel plate detector. In general, the time-averaged current of the (pulsed) beam was sufficiently large ($>10^{-14}$ A) for the current collected on the front surface of the channel plate (acting as a Faraday cup) to be recorded directly by an electrometer without amplification, thus avoiding the uncertainties inherent in the mass dependence of the channel plate detection efficiency. The largest clusters required amplification by the microchannel plate for detection. In these cases, care was taken to overlap a significant portion of the cluster mass range with both the unamplified and the amplified measurements to allow confident extrapolation of the microchannel plate detection efficiency to higher mass.

3. Results

3.1. $H_3^+(H_2)_n$

The cluster ion current, I_n^+, observed as a function of mass for hydrogen as the source gas is shown on a logarithmic intensity scale by the solid points in fig. 1. When this current is plotted as a function of the number n of neutral H_2 molecules attached to an H_3^+ core ion, two distinct regions are observed in which $\ln(I_n^+)$ decreases nearly linearly with n. These two regions, indicated by the solid lines in fig. 1, include the clusters $H_3^+(H_2)_n$, $n=1$–3 and $n=4$–6. The significance of these linear regions can be understood in terms of the structure of the cluster ions.

The structure of small hydrogen ion clusters has been extensively studied in both theory and exper-

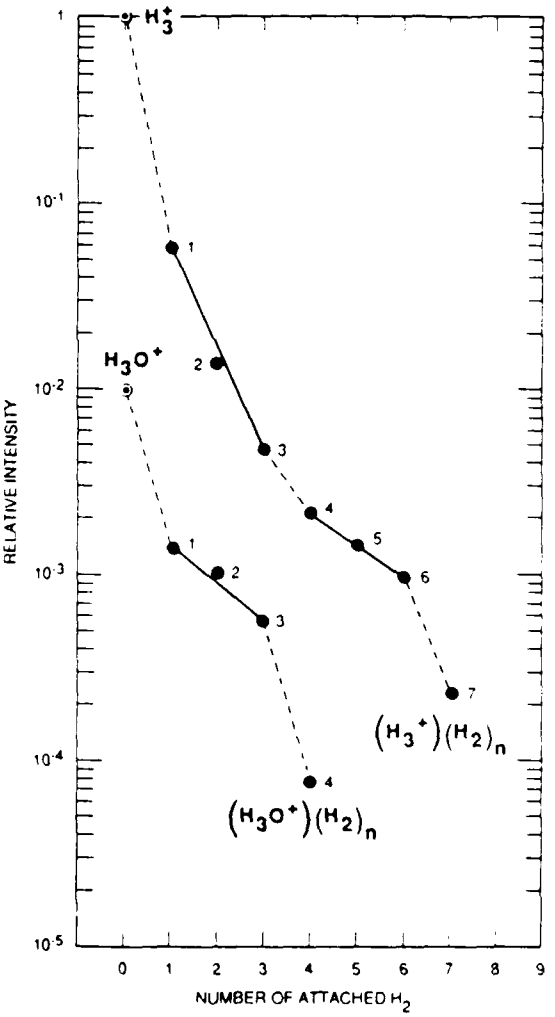

Fig. 1. Logarithmic intensity distribution of $H_3^+(H_2)_n$ and $H_3O^+(H_2)_n$ cluster ions.

iment [15–18]. The clusters are predicted to consist of a strongly bound, triangular H_3^+ core ion surrounded by more weakly bound H_2 molecules. These H_2 molecules are symmetrically positioned in two shells about the core. Following the notation of Amarouch, Durand, and Malrieu (ADM) [10], this shell structure can be described as (H_3^+, x, y), for $0 \leqslant y \leqslant x \leqslant 3$, where x designates the number of H_2 molecules occupying the shell closest to the core ion and y the number of these molecules in the next higher shell. In this notation, the two linear regions of ln (I_n^+) observed in fig. 1 encompass the cluster ion ranges $(H_3^+, 1, 0)$–$(H_3^+, 3, 0)$ and $(H_3^+, 3, 1)$–$(H_3^+, 3, 3)$, i.e. the decrease in this quantity remains nearly constant as equivalent H_2 molecules are added within each shell. However, the sharp decrease in intensity between $H_3^+ \cdot (H_2)_6$ and $H_3^+ \cdot (H_2)_7$ is difficult to understand in terms of the existing theoretical picture which predicts that H_{13}^+ has the closed-shell structure [17]. In the following sections we will present our data that indicate that in these ionic clusters the geometry with five neutrals almost equivalently attached to the core ion is very common. Using a similar picture one might speculate that the extra stability of the H_{15}^+ results from possible existence of an isomer structure that has pentagonal bipyramid geometry with H_5^+ (D_{2d} or D_{2h}) core ion [18]. Then, this possible isomer structure for H_{15}^+ can be described as $(H_5^+, 5)$ instead of $(H_3^+, 3, 3)$. Clearly further theoretical and experimental researches are needed to confirm the speculation.

3.2. $H_3O^+ \cdot (H_2)_n$

The $H_3O^+ \cdot (H_2)_n$ clusters were observed concurrently with the $H_3^+ \cdot (H_2)_n$ clusters due to a small impurity of water in the hydrogen source gas. The size dependence of the $H_3O^+ \cdot (H_2)_n$ cluster ion intensity, shown by the open points in fig. 1, is strikingly similar to that of $H_3^+ \cdot (H_2)_n$. The first linear region in the logarithm of cluster intensity occurs between $n=1$ and $n=3$, suggesting that these cluster ions have an H_3O^+ core ion [19,20] surrounded by H_2 molecules in a triangular shell structure, as is the case for $H_3^+ \cdot (H_2)_n$ ($n=1$–3), with the smaller slope of the linear region possibly indicating a weaker bond. A large intensity decrease accompanies the addition of the fourth H_2, suggesting the opening of the second shell. However, it was not possible to obtain data on the higher clusters due to their coincidence with other impurity ions in the present spectra.

3.3. $(CO)_n^+$

The most evident shell structure is seen for $(CO)_n^+$ cluster ions, as shown by the solid points in fig. 2. There is a discontinuous intensity decrease between the dimer ($n=1$) and trimer ($n=2$) ions. The first linear region appears between $n=3$ and 7, suggesting development of the first shell about a

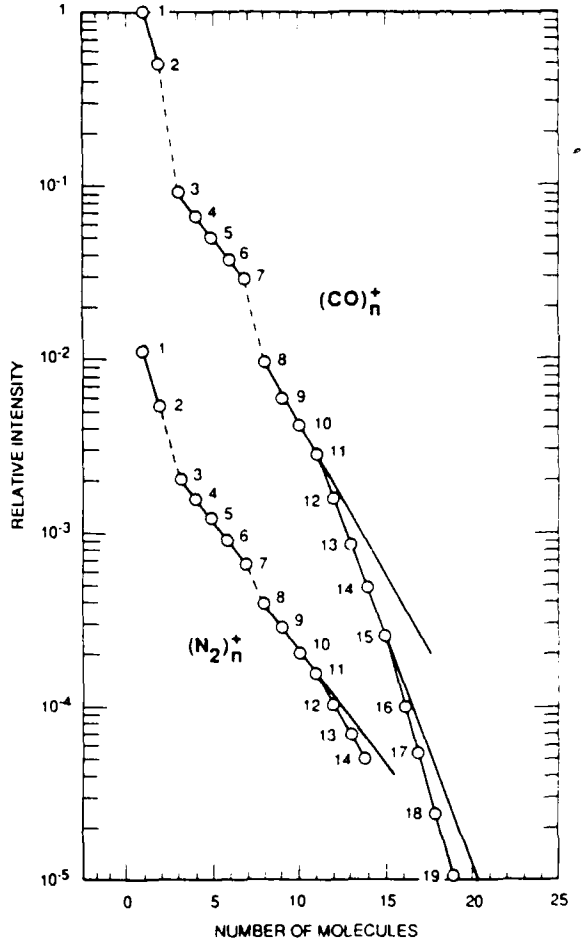

Fig. 2. Logarithmic intensity distribution of $(CO)_n^+$ and $(N_2)_n^+$ cluster ions. The evident structures between $n=3$ and $n=7$ are attributed to pentagonal bipyramid structures with dimer core ions.

$CO \cdot CO^+$ core ion. With a shell composed of five CO molecules, the most suggestive structure for $(CO)_7^+$ is a pentagonal bipyramid, with five polarized, neutral CO molecules around the dimer ion, or (2+, 5) using ADM's notation. This picture is consistent with our recent finding [12] that the wavelength dependence of the total photofragment cross sections of the $(CO)_3^+$ trimer ion is nearly identical to that observed [11] for the dimer ion, demonstrating that the addition of a CO molecule to the strongly bound dimer only weakly perturbs its electronic structure. A similar effect has been observed [6] for the addition of Ar to a core of Ar_3^+.

There are additional linear regions for $n=8$–11, and $n \geq 12$; however, the change in intensity between these regions is not large. In terms of a pentagonal bipyramid structure, completion of a second shell should require the addition of 10 CO molecules, leading to an expected onset of the third linear region at $n=18$, not $n=12$ as observed. From the computer simulation of the growth kinetics which will be presented in section 4, we tentatively conclude that the change is not caused by a change of the ion core but by limited growth of the larger ($n>11$) clusters owing to finiteness of the growth region in the ion source.

3.4. $(N_2)_n^+$

The intensity dependence observed for $(N_2)_n^+$ clusters is very similar to that of the isoelectronic $(CO)_n^+$ clusters. These data are given by the open circles in fig. 2. Here too, we suggest a pentagonal bipyramid structure about an N_3^+ core for clusters $(N_2)_n^+$ ($n \leq 7$). We note also that the break in the second linear region also occurs at $n=12$.

3.5. $(CO_2)_n^+$

The intensity dependence on cluster size for $(CO_2)_n^+$ is shown in fig. 3. In contrast to the other systems, the intensity dependence is nearly featureless, showing only a possible change in slope near $n=8$. Even the transition from dimer to trimer ion is accompanied by a relatively small intensity change. This may be a manifestation of the relatively weak bond of the $CO_2^+ \cdot CO_2$ dimer, approximately half that of $CO^+ \cdot CO$ [21], in comparison to the relatively

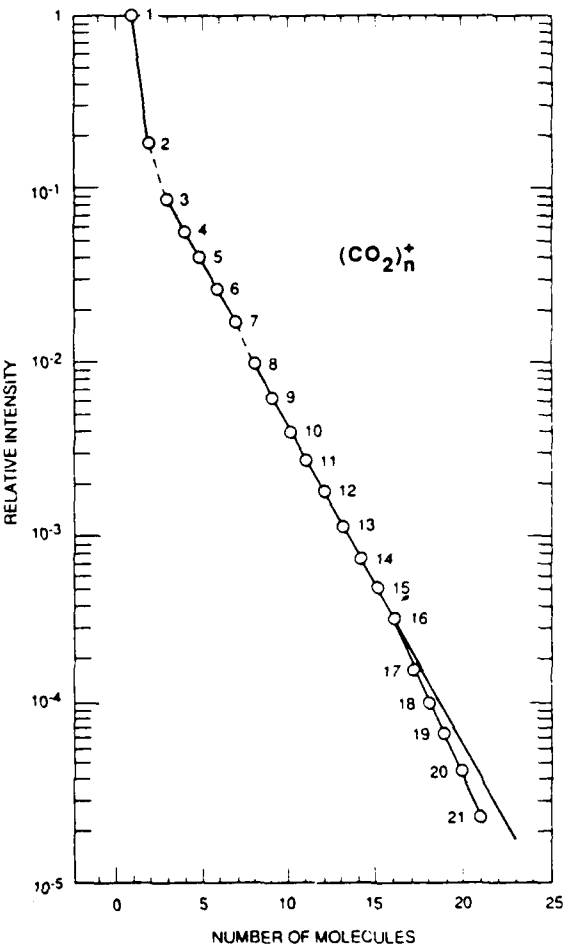

Fig. 3. Logarithmic intensity distribution of $(CO_2)_n^+$ clusters.

large polarizability of the CO_2 ligands, which is nearly twice that of CO [22]. On the basis of the intensity data, we would have to suggest a relatively amorphous structure for $(CO_2)_n^+$ clusters during the early stages of their growth.

3.6. Xe_n^+

The structure of Xe_n^+ cluster ions has recently been the subject of two detailed calculations [9,10]. These studies have found that for $n>5$, cluster growth is about a linear trimer ion core with the neutral atoms occupying radial positions in either of two five-membered "wheels" or "crowns", for which the trimer core serves as the "axle". In ADM's notation,

clusters $n \leqslant 13$ are represented $(3+, x, y)$, where x, $y \leqslant 5$. Since the wheels are occupied such as to maximize the distance between the neutral atoms, these two wheels can be considered a single shell containing a maximum of 10 atoms, for which we modify their notation to $(3+, x+y)$, $x+y \leqslant 10$. At $n=13$, the first shell is filled, forming a symmetric cluster $(3+, 10)$ with icosahedron structure about a trimer ion core. Above $n=13$, the core evolves into a linear, symmetric tetramer ion and at $n=19$ the second shell is completely filled to form a structure $(4+, 10, 5)$.

The intensity distribution that we observe for Xe_n^+ clusters is shown in fig. 4. The first linear region of $\ln(I_n^+)$ extends from $n=5$ to 12. Since a trimer ion core is predicted, one would expect a linear region beginning at $n=4$, yet the intensity change from $n=4$ to $n=5$ is somewhat larger than exponential, although it is a much smaller change than that which occurs between $n=3$ and $n=4$. This behavior is consistent with the prediction [9] of a linear tetramer structure for Xe_4^+ with a neutral Xe atom weakly bonded to a distorted trimer core ion, in contrast to the more strongly bound Xe atoms that occupy shells about the trimer ion core in clusters of higher n. It is also seen in fig. 4 that the intensity of $n=13$, completion of the first filled shell $(3+, 10)$, does not fall within the first linear region. Its higher intensity can be attributed to the increase in neutral Xe bond energy that is predicted [9,10] to accompany the formation of a symmetric Xe_{13}^+ icosahedron.

Above $n=13$, the intensity dependence of Xe_n^+ clusters cannot be described by linear regions. It is in this regime that theory predicts a transition to a tetramer core accompanied by a delocalization of core charge over the other atoms in the cluster [9]. The prominent intensities of $n=19$ and $n=25$, which together with $n=13$ have also been observed as magic numbers in other investigations [23–25], are consistent with the completion of shells $(4+, 10, 5)$ and $(5+, 10, 5, 5)$, respectively. It is noteworthy that addition of a Xe atom to each of these filled-shell cluster ions is manifested by a large decrease in the intensity of the product cluster. However, the largest intensity decrease is observed between $n=13$ and $n=14$, reflecting the substantial cluster rearrangement that must accompany the core conversion $(3+, 10) \rightarrow (4+, 10)$.

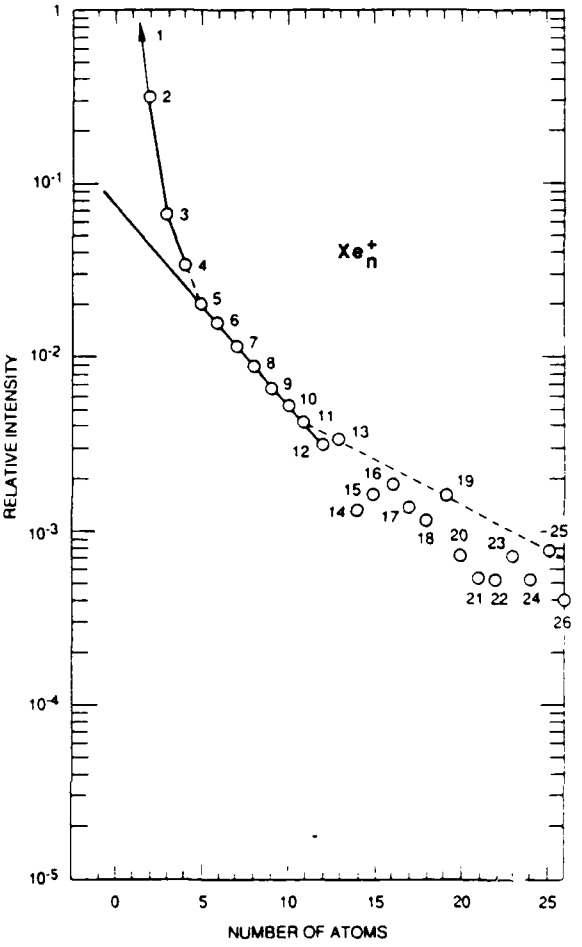

Fig. 4. Logarithmic intensity distribution of Xe_n^+ clusters. The intensity enhancement at $n=13$, 19, and 25 can be attributed to completion of shells $(3+, 10)$, $(4+, 10, 5)$ and $(5+, 10, 5, 5)$ with elongated icosahedral structures respectively.

4. Discussion

A notable success of cluster ion research has been the finding that the ionic charge (electron hole) is not delocalized over the cluster as in the case of metallic cluster, but principally resides in the core ion [9]. Bonding of the molecular shells to the core in small clusters occurs mainly through polarization forces. It is likely that the regions of near-exponential decrease observed in the cluster ion intensity are a manifestation of the nearly equal degrees of shielding of the core charge experienced by molecules

within each shell. In addition the large abrupt breaks in intensity at particular n suggest significant changes in the growth rate that is related to the structure of the cluster ions. In this particular experiment the conditions were such as to provide ideal growth conditions that permit a simple model to be formulated. It is notable that the primary ion is the dominant ion since the sum of the rest of the ions produced is less than 50% of the primary ion intensity and thus all of the larger clusters are still growing as the beam exits the growth region. This suggests a simple model that assumes the clusters grow stepwise by adding a single ligand at a time. The model, in its most simplistic form, assumes that the primary ion is injected into a volume of gas (the expansion gas) and is depleted by molecular capture that produces a dimer ion which subsequently captures another molecule to become a trimer and so on until the ions exit from the region of growth. Thus all of the ions are growing as a function of distance as they pass through the slug of gas. The cluster ions are expected to be formed in three-body association reactions:

$$X^+ \cdot Y_n + Y + Y \rightarrow X^+ \cdot Y_{n+1} + Y\,, \qquad (1)$$

where X^+ is the core ion for the shell. We believe the formation of the stable cluster ions occurs through two steps: the formation of long-lived states of which lifetimes greater than or equal to the collision time and the collisional quenching of the states into stable ones [21]. Then, the rate constant K_{n+1} for the formation of n cluster ions is a function of both capturing and quenching cross sections as well as the lifetime of the intermediate complex.

Applying this model the growth curves can be computed by solving the set of differential equations

$$dI_i/dx = I_{i-1}K_{i-1} - I_iK_i\,, \quad i = 1-n \qquad (2)$$

for the applicable range of i. Here in this crude model the beam scattering processes that would remove intensity from the beam are ignored. These processes are likely to be most effective with the light ions at the beginning of the growth cycle.

We attempted to simulate $(CO)_n^+$ intensity curves by numerically solving eq. (2), adjusting the K_i to give qualitative reproduction of the experimental results. Since the gas slug geometry is poorly defined and the density in the jet is not well known, no attempt is made to extract cross sections. Here the exit point is chosen at the point where the intensity of $(CO)_2^+$ has grown to 50% of the monomer ion as is observed in the results. At this point the growth is stopped and the intensities are plotted as a function of n. Such a plot is shown in fig. 5. The nearly linear portions of the $\ln(I_n)$ plot occur for groups of clusters having the same K_i with breaks occurring when K_i changed significantly. For example, the break between $i=7$ and 8 resulted from a factor of 2.5 reduction of the rate constant at $i=7(K_7)$ producing a bottleneck for forming $(CO)_8^+$. Thus the model clearly supports the interpretation that the breaks in the curves are associated with the cluster shell structure. The filling shell is associated with a nearly constant formation rate and a filled shell appears as a sudden decline in the rate. Thus the experimental conditions used here of growing the clusters from monomer ions provides a simple means for exploring structural aspects of the clusters as they are reflected in the growth mechanisms. The faster than linear trend in $\ln(I_n)$ for $n>8$ is predicted by the model for a constant rate. We also found that a similar model can be applicable to the $(N_2)_n^+$ cluster ions.

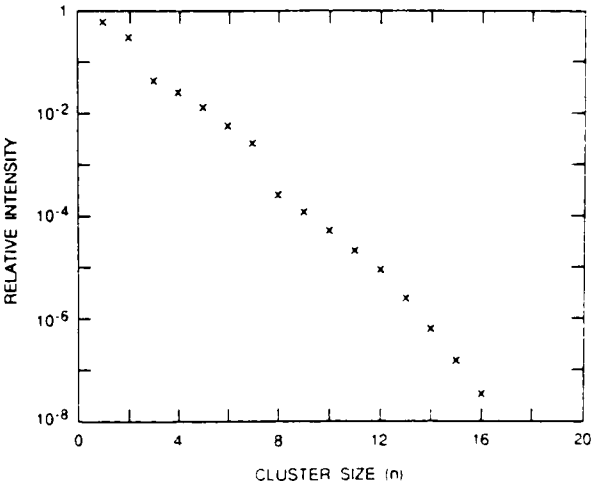

Fig. 5. Computer simulation result of $(CO)_n^+$ and $(N_2)_n^+$ clusters by solving eq. (2). The rate constants are set equal in each shell ($1 \leq n \leq 2$, $3 \leq n \leq 7$, and $8 \leq n$).

5. Conclusion

We have found that the variation in the logarithm of cluster ion abundance as a function of cluster size for the case of $H_3^+ \cdot (H_2)_n$ is highly correlated with known variations in the structure of these clusters and associate linear regions in this variation with the addition of equivalent H_2 molecular ligands to an ionic core of particular structure. Similar variations are observed in the abundances of $H_3O^+ \cdot (H_2)_n$ ($n \leqslant 4$), $(CO)_n^+$ ($n \leqslant 19$), $(N_2)_n^+$ ($n \leqslant 14$), and $(CO_2)_n^+$ ($n \leqslant 16$) clusters. We have proposed structures for both the ionic core and the placement of the molecular ligands in these clusters, which agree with previous experimental and the oretical data, when available. Minor deviations in the correlation of cluster abundance with structure are observed for the rare gas cluster Xe_n^+ ($n \leqslant 26$). These deviations are associated with significant changes in the structural symmetry of the rare gas cluster during its growth, implying that symmetry plays a larger (or smaller) role in the growth of molecular cluster ions. It should be emphasized that the present assignments may not be unique, but they provide a good starting point for further experimental investigation.

Acknowledgement

This research was supported by the Independent Research and Development Program of SRI International and by the Air Force Astronautics Laboratory (Contract F04611-87-C-0025). We acknowledge very helpful and stimulating discussions with Drs. G.P. Smith and D.L. Huestis during the course of this work and gratefully acknowledge the technical contributions of M. Nicholson, W. Olson, and S. Young to construction of the apparatus.

References

[1] J. Jortner, Ber. Bunsenges. Physik. Chem. 88 (1984) 188.
[2] J.C. Phillips, Chem. Rev. 86 (1986) 619.
[3] A.L. Mackay, Acta Cryst. 15 (1962) 916.
[4] M.R. Hoare and P. Pal, Nature 236 (1972) 35.
[5] M.L. Alexander, M.A. Johnson, N.E. Levinger and W.C. Lineberger, Phys. Rev. Letters 57 (1986) 976.
[6] N.E. Levinger, D. Ray, M.L. Alexander and W.C. Lineberger, J. Chem. Phys. 89 (1988) 5654.
[7] N.E. Levinger, D. Ray, K.K. Murray, A.S. Mullin, C.P. Schulz and W.C. Lineberger, J. Chem. Phys. 89 (1988) 71.
[8] H. Haberland, in: Electronic and atomic collisions, eds. J. Eichler, I. Hertel and N. Stolterfoht (North-Holland, Amsterdam, 1984) p. 597.
[9] P.J. Kuntz and J. Valldorf, Z. Physik D 8 (1988) 195.
[10] M. Amarouche, G. Durand and J.P. Malrieu, J. Chem. Phys. 88 (1988) 1010.
[11] S.C. Ostrander, L. Sanders and J.C. Weisshaar, J. Chem. Phys. 84 (1986) 529.
[12] Y.K. Bae and P.C. Cosby, unpublished.
[13] M.A. Johnson, M.L. Alexander and W.C. Lineberger, Chem. Phys. Letters 112 (1984) 285.
[14] Y.K. Bae and P.C. Cosby, Rev. Sci. Instr., submitted for publication.
[15] K. Hiraoka, J. Chem. Phys. 87 (1987) 4048.
[16] M. Okumura, L.I. Yeh and Y.T. Lee, J. Chem. Phys. 88 (1988) 79.
[17] K. Hirao and S. Yamabe, Chem. Phys. Letters 80 (1983) 237.
[18] Y. Yamaguchi, J. Gaw and H.F. Schaefer III, J. Chem. Phys. 78 (1983) 4074.
[19] D.J. Liu and T. Oka, Phys. Rev. Letters 54 (1985) 1787.
[20] P. Botschwina, J. Chem. Phys. 84 (1986) 6523.
[21] C.Y. Ng, Advan. Chem. Phys. 52 (1983) 363.
[22] T.M. Miller, in: CRC handbook of chemistry and physics, ed. R.C. Weast (CRC Press, Boca Raton, 1988) E-66.
[23] I.A. Harris, R.S. Kidwell and J.A. Northby, Phys. Rev. Letters 53 (1984) 2390.
[24] O. Echt, K. Sattler and E. Recknagel, Phys. Rev. Letters 47 (1981) 1121.
[25] D. Kreisle, O. Echt, M. Knapp and E. Recknagel, Phys. Rev. A 33 (1986) 768.
[26] B.M. Smirnov, Soviet Phys. Usp. 20 (1977) 119.

APPENDIX C

ARE THE GEOMETRICAL STRUCTURES OF H_{15}^{+} AND H_{27}^{+} A PENTAGONAL BIPYRAMID AND AN ICOSAHEDRON?

ARE THE GEOMETRICAL STRUCTURES OF H_{15}^+ AND H_{27}^+ A PENTAGONAL BIPYRAMID AND AN ICOSAHEDRON?

Young K. Bae
Molecular Physics Laboratory
SRI International
Menlo Park, CA 94025

ABSTRACT

The structures of H_{2n+1}^+ ($n \geq 5$) cluster ions are suggested to be strongly influenced by competition of positive charge delocalization and ion-neutral polarization in the clusters. Based on the experimentally observed stability, the geometrical structure of H_{15}^+ is suggested to be a pentagonal bipyramid with the H_5^+ core ion surrounded by one 5 H_2 crown. The extra stability of H_{27}^+ observed by van Lumig and Reuss is correlated with a deformed icosahedron with the H_7^+ core ion surrounded by two 5 H_2 crowns. The possible growth paths, structures, and related stability of other H_{2n+1}^+ cluster ions up to n = 13 are also suggested.

MP 90-058
March 22, 1990

The properties of the hydrogen cluster ions which are the most fundamental cluster ions have been of great experimental and theoretical interest. Current ab initio theoretical studies[1,2] predict that geometries of the H_{2n+1}^+ cluster ions are dominated by the equilateral triangular geometry of the H_3^+ core ion; H_9^+ forms the first shell with three H_2 molecules attached to the apexes of H_3^+, and H_{13}^+ forms the second shell with additional two H_2 molecules attached to the top and bottom of the triangular plain formed by H_9^+. Although both experimental[3-5] and theoretical[1,2] results agree with the stability of H_9^+, it seems that the theoretically predicted structures[1] with the H_3^+ core do not explain various experimental results for clusters larger than H_9^+. Recently we have observed shell structures manifested in the size distributions of various non-metallic cluster ions.[3] The results showed a sharp decrease in the intensity distribution of H_{2n+1}^+ between H_{15}^+ and H_{17}^+ indicating that H_{15}^+ forms the closed shell structure. More than 10 years ago, in their collisional fragmentation study of H_{2n+1}^+ up to H_{41}^+ van Lumig and Reuss found that the fragmentation channels producing H_9^+, H_{15}^+, and H_{27}^+ have larger cross sections than their respective neighbors and concluded that these cluster ions are particularly stable.[4] They also noted that H_{19}^+ and H_{23}^+ are relatively more stable than their neighbors. Hiraoka measured equilibria of clustering reaction $H_{2n+1}^+ + H_2 = H_{2n+1}^+$ and found that H_5^+, H_9^+, H_{15}^+, and H_{19}^+ are relatively more stable toward dissociation compared to their neighbors.[5] Thus, these experimental results[3] show apparent stability of H_{15}^+, indicating that it might form a stable closed shell structure. Furthermore, the extra stability of H_{27}^+ and relative stability of H_{19}^+ and H_{23}^+ can not easily be understood in terms the structures with the H_3^+ core ion.

Very recent theoretical studies[6,7] with the diatomics-in-molecules (DIM) method have shown that the structures of small nonmetallic positive ion clusters are mainly determined by competition between two major interactions in cluster ions: charge delocalization and ion-neutral polarization. In this picture the positive charge (electron hole) is not delocalized all over the cluster ion as in the case of metallic clusters, but mainly resides in a core ion. The cluster shells are formed by bonding neutral polarized moieties to the core ion through polarization forces.

The results of our experimental study[3] on various cluster ions are consistent with this picture. The intensity distribution of the mass spectra indicated that in some ion clusters such as $(CO)_n^+$, the positive charge is localized only in the dimer, but in others such as Xe_n^+ the charge seems to propagate linearly over many atom distances, forming a long linear core ion. These experimental findings are consistent with the theoretical prediction that a dimer core ion can have one crown which can bear up to five moieties, a trimer can support two crowns, and so forth.[6,7] With this picture we suggested[3] that the structures of $(CO)_7^+$ and $(N_2)_7^+$ are pentagonal bipyramids with dimer core ions surrounded by five polarized neutral molecules. A schematic representation of the structure is shown in Figure 1a. In the figure the black core represents the charged core ion and the white balls represent the polarized neutral moieties. It is interesting to note that similar pentagonal bipyramidal structures have been predicted for the $Br_2^-(CO_2)_5$ cluster ion using molecular dynamics calculations.[8]

Theoretical calculations[9] predict that the potential surface of the D_{2d} H_5^+ geometry lies only 30 cm^{-1} above the global minimum C_{2v} geometry, indicating that the two geometries are virtually indistinquishable in actual experiments. The C_2 geometry has the charge more localized in one H_2 molecule forming a distorted H_3^+, whereas the D_2 has geometry has the charge equally shared by the two H_2 molecules forming a proton bound dimer $H_2 \bullet H^+ \bullet H_2$. It seems possible that the H_7^+ and H_9^+ cluster ions might have isomers with two different core ions: H_3^+ and H_5^+. What would be the core ions for the cluster ions larger than H_9^+? Based on the "core ion + five member crowns" structures as observed in various other cluster ions, I propose here that the experimentally observed stability of the H_{15}^+ is correlated with a pentagonal bipyramid structure which has the H_5^+ core with a geometry possibly like the D_{2d} structure. With the notations of Amarouch, Durand, and Malrieu (ADM),[6,3] H_{15}^+ is then described as $(H_5^+,5)$. A schematic representation of this structure is shown in Figure 1a. Here the black core represents H_5^+ and the white balls represent the H_2 molecules.

If the H_{15}^+ has the H_5^+ core ion, can the charge be further delocalized to form a larger ion

core? It seems that such charge delocalization might play a key role in determining the stability and growth paths of the larger H_{2n+1}^+ cluster ions. If the charge is further delocalized beyond the H_5^+ core ion to form an almost linear H_7^+ core ion (possibly a deformed C_{2v} structure with the flattened H_3^+ triangle) which can have two crowns (ten H_2 molecules), then H_{27}^+ is predicted to form the next complete shell structure, thus to be very stable. Evidence for this structure comes from the extra stability of H_{27}^+ observed by van Lumig and Reuss[4] extra stability of the H_{27}^+ in their collisional dissociation study of hydrogen cluster ions. The extra stability of the H_{27}^+ might result from a deformed icosahedral structure in which two five-H_2 molecule crowns surround an H_7^+ core ion, (H_7^+,5,5), which is similar to that predicted for Xe_{13}^+.[3,6] A schematic representation of this structure is shown in Figure 1b. Here the dark core represents H_7^+ and the white balls represent the H_2 molecules.

Considering the proposed structures of H_{15}^+ and H_{27}^+, one can predict possible structures of the H_{2n+1}^+ cluster ions up to H_{27}^+ which are summarized in Table 1 and described using the ADM notations. Figure 2 and 3 show the schematic representations for the proposed structures. It is very interesting to note that both H_{19}^+ and H_{23}^+ can have structures with higher symmetry (H_7^+,3,3) and (H_7^+,4,4), respectively, thus can be relatively stable compared with their neighbors. Indeed van Lumig and Reuss[4] also observed that H_{19}^+ and H_{23}^+ are relatively more stable than their neighbors. Thus, it is possible that the experimentally observed relative stability of H_{19}^+ and H_{23}^+ might result from these geometries with higher symmetry. The smaller cluster ions H_7^+ and H_9^+ might have two isomers with two different core ions, H_3^+ and H_5^+. If the proposed structures for the clusters larger than H_9^+ are correct, only the isomers with the H_5^+ cores are likely to evolve to the larger clusters.

Okumura et al.[10] measured vibrational frequencies of the H_2 stretching mode in H_{2n+1}^+ clusters up to n = 7. They found that the H_2 frequencies in the cluster ions are considerably red-shifted compared to the H_2 frequency in gas phase. For H_5^+, the red-shift was as much as 250 cm^{-1}. As the cluster size increased, the red-shifts decreased monotonically to 140 cm^{-1} for

H_9^+; however, after H_9^+, the frequency shift changed only little, from 140 cm^{-1} to 115 cm^{-1}. Thus, the results supported the model of H_9^+ as an H_3^+ with three H_2 molecules attached to the apexes.[10] They also found that the absorption bands of the H_2 stretching mode for the clusters larger than H_9^+ show less red-shifted weak shoulders beside the main band peaks, whereas those for smaller clusters did not. We suppose that if the main peak resulted from H_5^+ and if the weak shoulders from an H_2 molecule in the crowns, then the absence of weak shoulders in the spectra of the smaller ones might indicate that the populations of structures with the H_3^+ core were much higher than those with the H_5^+ core in the ion beams of H_7^+ and H_9^+ used for their experiment. According to the proposed model, clusters larger than H_9^+, however, have only the H_5^+ core, thus are expected to show more distinct weak shoulders in the absorption spectra as seen in their results.

These proposed growth paths and structures are logically appealing but are, of course, speculative. The structure of clusters will also depend on their internal temperatures. Because most of the cluster ion beams were observed to undergo metastable decay,[3,11] it is possible (and reasonable) that the experimentally generated cluster ions have a range of internal temperatures. Thus, the proposed structures might characterize clusters with a range of internal temperatures. More experimental and theoretical studies on the hydrogen cluster ions are clearly needed.

Very helpful and stimulating discussions of Drs. H. Michels, H. Helm, P. C. Cosby, J. R. Peterson, and R. P. Saxon, and the support of the Air Force Astronautics Laboratory (Contract F04711-87-C-0025) are greatly acknowledged.

REFERENCES

1. K. Hirao and S. Yamabe, Chem. Phys. Lett. **80**, 237 (1983).

2. Y. Yamaguchi, J. F. Gaw, and H. F. Schaefer III, J. Chem. Phys. **78**, 4047 (1983).

3. Y. K. Bae, P. C. Cosby, and D. C. Lorents, Chem. Phys. Lett. **159**, 214 (1989).

4. A. van Lumig and J. Reuss, Int. J. Mass. Spect. Ion. Phys. **11**, 483 (1978).

5. K. Hiraoka, J. Chem. Phys. **87**, 4048 (1987).

6. M. Amarouche, G. Durand, and J. P. Malrieu, J. Chem. Phys. **88**, 1010 (1988).

7. J. Hesslich and P. J. Kuntz, Z. Phys. D **2**, 251 (1988).

8. L. Perera and F. G. Amar, J. Chem. Phys. **90**, 7354 (1989).

9. Y. Yamaguchi, J. F. Gaw, R. B. Remington, and H. F. Schaefer III, J. Chem. Phys. **86**. 5072 (1987).

10. M. Okumura, L. I. Yeh, and Y. T. Lee, J. Chem. Phys. **88**, 79 (1988).

11. J. Kirchner and M. T. Bowers, J. Phys. Chem. **91**, 2573 (1987).

FIGURE CAPTION

Figure 1 a) A schematic representation for the pentagonal bipyramidal structures of H_{15}^+, $(CO)_7^+$, and $(N_2)_7^+$. The black core represents H_5^+, $(CO)_2^+$ and $(N_2)_2^+$, whereas the white balls represent H_2, CO, and N_2 molecules, respectively.

b) A schematic representation for the deformed icosahedral structures of H_{27}^+ and Xe_{13}^+.

The black cores are the core ions (H_7^+ and Xe_3^+) and the white balls are the neutral moieties (H_2 and Xe).

Figure 2. Schematic representations for H_{2n+1}^+ clusters up to H_{15}^+. The black cores are core ions. The white balls are the H_2 molecules.

Figure 3. Schematic representations for H_{2n+1}^+ clusters up to H_{27}^+. The black cores are core ions. The white balls are the H_2 molecules. Note that H_{19}^+ and H_{23}^+ can have the higher symmetry structures, (H_7^+,3,3) and (H_7^+,4,4), respectively.

TABLE 1

Proposed growth paths of odd-numbered hydrogen cluster ions.

Cluster Ion	Proposed Structures in ADM notation
H_3^+	$(H_3^+,0)$
H_5^+	$(H_3^+,1)$, $(H_5^+,0)$
H_7^+	$(H_3^+,2)$, $(H_5^+,1)$
H_9^+	$(H_3^+,3)$, $(H_5^+,2)$
H_{11}^+	$(H_5^+,3)$
H_{13}^+	$(H_5^+,4)$
H_{15}^+	$(H_5^+,5)$ -- Pentagonal Bipyramid
H_{17}^+	$(H_7^+,5,0)$, $(H_7^+,4,1)$, $(H_7^+,3,2)$
H_{19}^+	$(H_7^+,5,1)$, $(H_7^+,4,2)$, $(H_7^+,3,3)$
H_{21}^+	$(H_7^+,5,2)$, $(H_7^+,4,3)$
H_{23}^+	$(H_7^+,5,3)$, $(H_7^+,4,4)$
H_{25}^+	$(H_7^+,5,4)$
H_{27}^+	$(H_7^+,5,5)$ -- Icosahedron

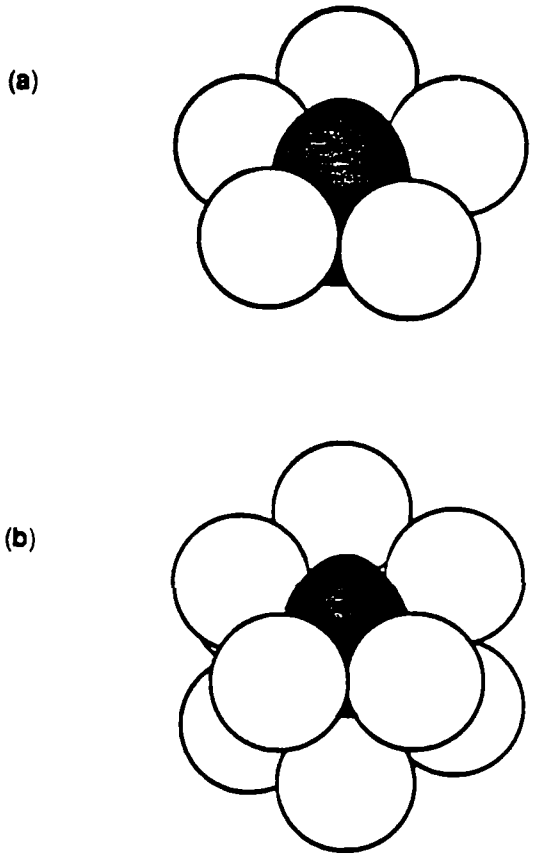

Figure 1

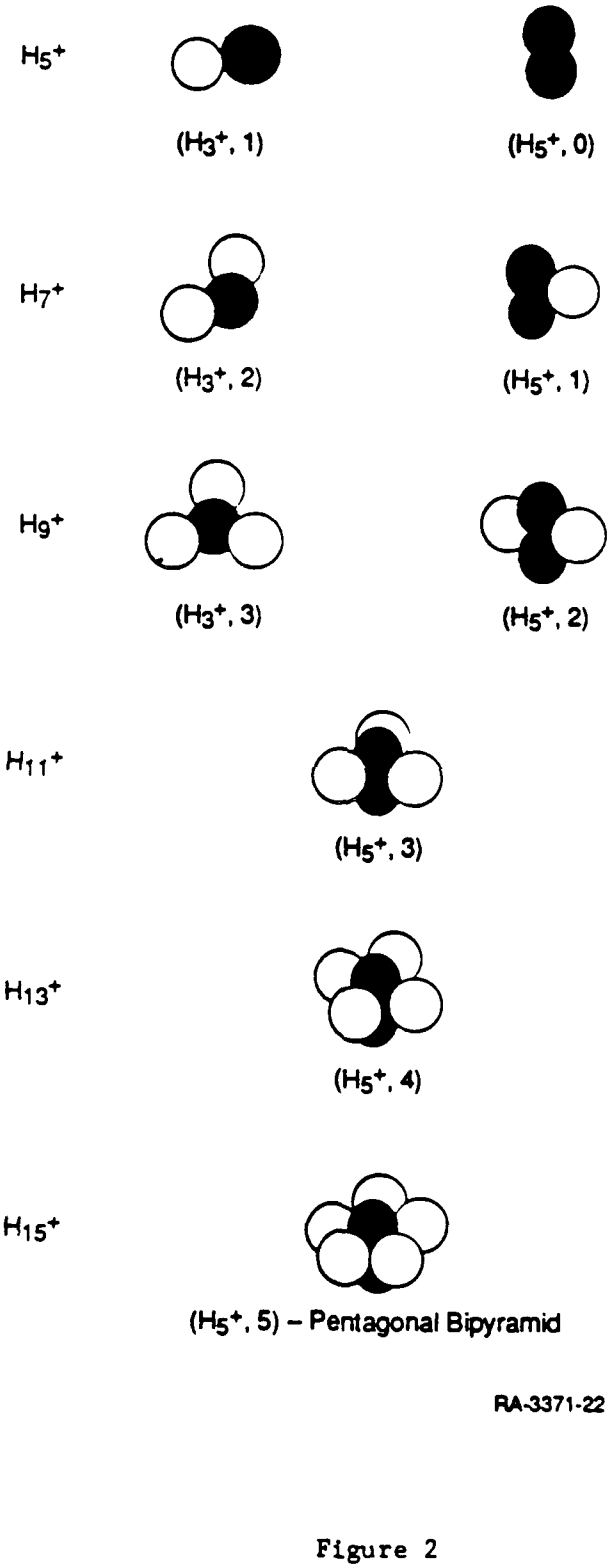
H_5^+
$(H_3^+, 1)$
$(H_5^+, 0)$
H_7^+
$(H_3^+, 2)$
$(H_5^+, 1)$
H_9^+
$(H_3^+, 3)$
$(H_5^+, 2)$
H_{11}^+
$(H_5^+, 3)$
H_{13}^+
$(H_5^+, 4)$
H_{15}^+
$(H_5^+, 5)$ – Pentagonal Bipyramid
RA-3371-22

Figure 2

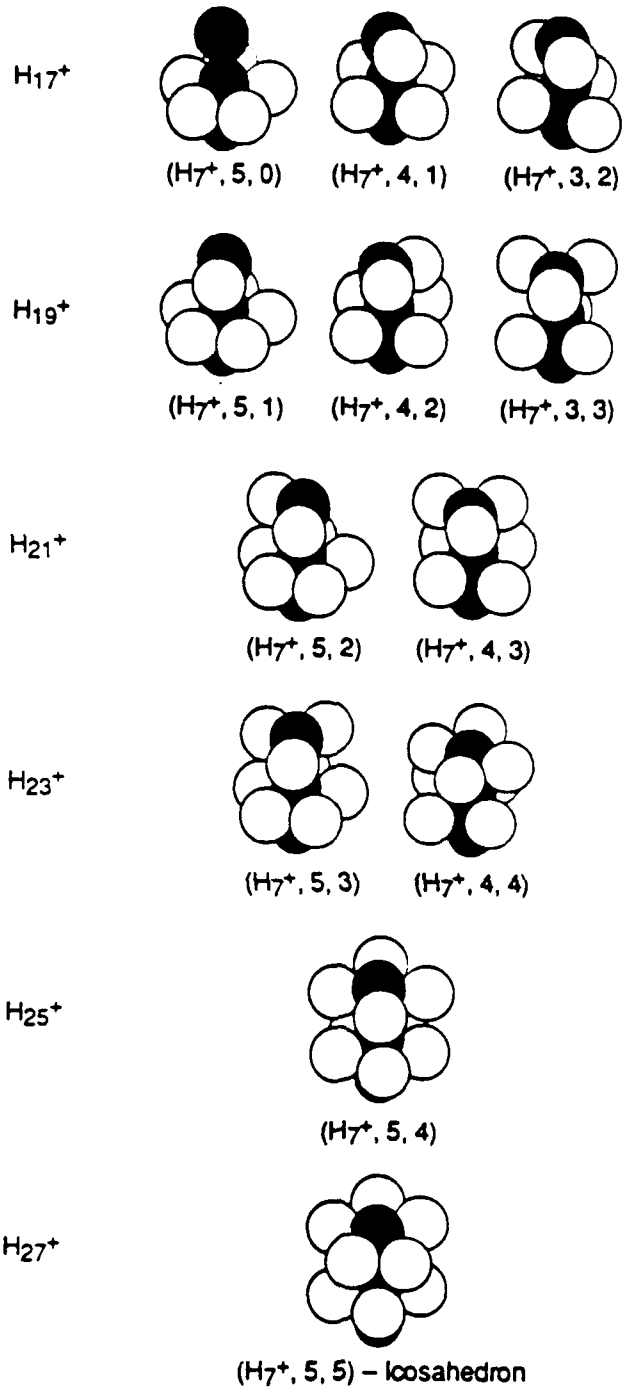
H_{17}^+
$(H_7^+, 5, 0)$
$(H_7^+, 4, 1)$
$(H_7^+, 3, 2)$
H_{19}^+
$(H_7^+, 5, 1)$
$(H_7^+, 4, 2)$
$(H_7^+, 3, 3)$
H_{21}^+
$(H_7^+, 5, 2)$
$(H_7^+, 4, 3)$
H_{23}^+
$(H_7^+, 5, 3)$
$(H_7^+, 4, 4)$
H_{25}^+
$(H_7^+, 5, 4)$
H_{27}^+
$(H_7^+, 5, 5)$ – Icosahedron
RA-3371-23

Figure 3

APPENDIX D

OBSERVATION OF BOUND-FREE PHOTODISSOCIATION OF H_3^+

REPRINTED WITH PERMISSION

PHYSICAL REVIEW A VOLUME 41, NUMBER 3 1 FEBRUARY 1990

Observation of bound-free photodissociation of H_3^+

Y. K. Bae and P. C. Cosby
Molecular Physics Laboratory, SRI International, Menlo Park, California 94025
(Received 7 November 1989)

We have observed a bound-free photodissociation of H_3^+ caused by a single-photon absorption from highly excited rovibrational levels of the H_3^+ ground state into the continuum of the first-excited singlet electronic state. The apparent threshold energy of the dissociation has been measured to be -2.5 eV, in agreement with the calculated one by Talbi and Saxon [D. Talbi and R. Saxon, J. Chem. Phys. **89**, 2235 (1988)].

There has been extensive theoretical and experimental work on the H_3^+ molecule because of its practical and fundamental importance.[1-4] This ion plays an important role in understanding the properties of H_{2n+1}^+ cluster ions, which are believed to be described as H_3^+ surrounded by $n-1$ H_2 molecules.[5-7] The structure of H_3^+ and its isotopomers has been successfully probed in a variety of experiments encompassing infrared absorption,[8,9] beam-foil spectroscopy,[10] translational spectroscopy,[11] and vibrational predissociation.[12] This work, however, has explored only the ground electronic state of the ion, labeled $1\,^1A_1'$ or $1\,^1A'$ in D_{3h} or C_{2v} symmetry, respectively. Other electronic states are known only from quantum chemistry calculations.[13-17] When accessed at the equilibrium geometry of the ground electronic state, these excited electronic states are expected to lie prohibitively high in energy for optical excitation. Only a single experiment, electron-impact dissociation to form protons,[18] has suggested accessing any excited state of H_3^+.

We report here the first observation of the reaction:

$$H_3^+ + h\nu \rightarrow H_2^+ + H, \qquad (1)$$

which we interpret as occurring in a bound-free, single-photon absorption from highly excited rovibrational levels of the H_3^+ ground state into the continuum of the first-excited singlet electronic state. Details of the experimental apparatus are given elsewhere.[19] The H_3^+ are generated by 200-eV electron impact near the nozzle of a pulsed, supersonic expansion of room-temperature H_2 gas. Ions are extracted coaxially from the expansion through a skimmer by a weak (1 V/cm) electric field, accelerated to 3 keV, and mass selected by a 60° magnetic sector to produce an H_3^+ beam composed of 200 μs full width at half maximum pulses with peak currents of 200 nA. The collimated H_3^+ beam is overlapped over a distance of 60 cm by a laser beam. Charged dissociation products produced in this region are selected in energy (mass) by an electrostatic energy analyzer and detected by a microchannel plate electron multiplier. Photons were generated by the fundamental and second harmonic of a yttrium aluminum garnet (YAG)-pumped dye laser, operated synchronously at 10 Hz with the pulsed ion beam.

When irradiated by the laser at wavelengths below 5000 Å, the H_3^+ ions photodissociated to form H_2^+ [reaction (1)]. The yield of H_2^+ products was found to be linear in photon flux over the laser pulse energy range of 0.2–2.0 mJ at several wavelengths above the threshold, suggesting a single-photon photodissociation process. In contrast, production of H^+ fragments, the lowest-energy dissociation channel, was negligible at all wavelengths and photon fluxes investigated. The relative yield of H_2^+ photofragments, normalized to constant laser power, is shown in Fig. 1 as a function of photon energy. Above the apparent threshold near 2.5 eV, the yield of H_2^+ increases rapidly with photon energy. At a photon energy of 4.0 eV, we estimate the apparent cross section for the photodissociation to be 10^{-22} cm^2. This small value suggests either a highly unfavorable photoabsorption process or the participation of only a small fraction of the H_3^+ ions in the reaction.

We first considered the contribution to the observed signal from photodissociation of HD^+ as an impurity at the natural abundance level (330 ppm of H_2^+) in the H_3^+ beam. The resolution of the primary mass selector is too low to separate HD^+ from H_3^+ and the photofragments from each species are effectively indistinguishable in energy. We exclude HD^+ as a major contributor to the fragment yield because photodissociation of D_3^+, which is uncontaminated by isotopic impurities, was found to have a

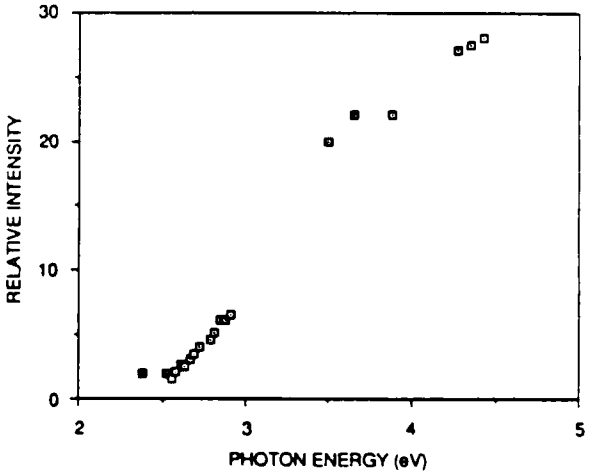

FIG. 1. Relative H_2^+ (mass is equal to 2 amu) photofragment yield from the photodissociation of H_3^+ as a function of laser photon energy. H^+ photofragment yields from H_3^+ are found to be negligible.

D_2^+ product yield at 3.5-eV photon energy that is essentially identical to the H_2^+ yield from H_3^+. As a second test, the photodissociation of H_2^+, which should behave similar to HD^+, was observed over the range of photon energies employed here. The H^+ photofragment yield was found to be essentially wavelength independent. When this yield is scaled to the abundance of HD^+ in the H_3^+ beam, D^+ photofragments from HD^+ are projected to make an insignificant contribution to the data in Fig. 1 at photon energies above 2.7 eV, but likely account for the small photofragment yield at and below the 2.5-eV threshold.

The proposed mechanism for the photodissociation of H_3^+ is illustrated in Fig. 2. The potential energy curves of the ground electronic state of H_3^+ and the first-excited singlet state, labeled $1\,^1A'$ and $2\,^1A'$ in C_s symmetry, are taken from Table III of Talbi and Saxon.[17] In their tabulation, the energy at the C_{2v} dissociation asymptote represent production of the diatomic product (H_2 or H_2^+) at the equilibrium internuclear separation of H_2 (0.741 Å). At this separation, the H_2 molecule is at its potential minimum, whereas H_3^+ has a potential energy roughly corresponding to two quanta of vibrational excitation. To account for the requisite zero-point vibrational energy[20] in the H_2, we have uniformly shifted the $1\,^1A'$ potential energy by 0.27 eV. No attempt is made to account for the zero-point energy[21] of H_3^+ at small R. It can be seen from Fig. 2 that the vertical excitation energy for the $2A'$-$1\,^1A'$ transition, calculated to be 19.325 eV at the equilibrium geometry of the ground state, decreases to roughly 2.5 eV as one of the nuclei is separated from the remaining two, such as occurs along the asymmetric stretch coordinate during vibration. The vertical arrows in Fig. 2 represent the excitation energies equivalent to the observed photodissociation threshold and the highest photon energy. Agreement with the calculated vertical excitation energies is striking, suggesting that the initial states probed in reaction (1) are highly excited vibrational levels of the ground electronic state lying ≤ 1 eV below the $H^+ + H_2$ ($v = 0$) dissociation asymptote.

We can reasonably expect excited vibrational levels to be populated in the H_3^+ ion beam. Electron impact on pure H_2 gas in the ion gives rise to H_2^+ ions which undergo the rapid reaction

$$H_2^+ + H_2 \rightarrow H_3^+ + H . \qquad (2)$$

The high exothermicity of (2) yields H_3^+ in a wide range of excited rovibrational levels.[22] Carrington and Kennedy[12] have observed numerous vibrational predissociation transitions originating in H_3^+ rovibrational levels, populated via (2), that lie within 0.12 eV of the dissociation asymptote. Cooling of this excitation by subsequent collisions in the source expansion also promotes the growth of $H_3^+(H_2)_n$ ($n = 1$–7) clusters,[23] which account for only 10% of the total ion flux under the conditions of the present experiment. We therefore expect most of the nascent excitation to be retained by H_3^+ ions extracted from the source.

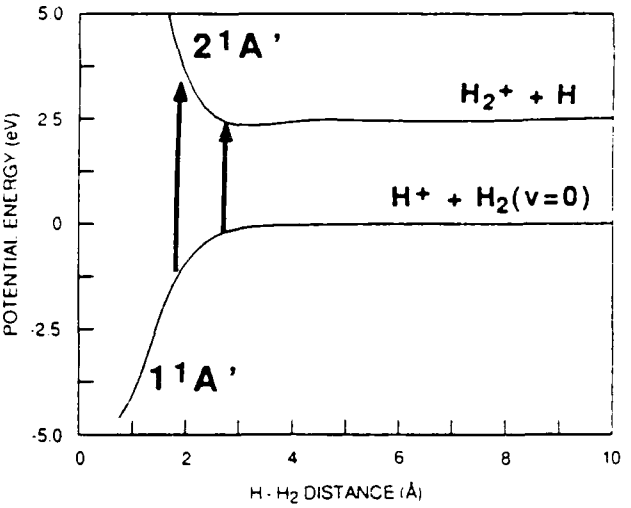

FIG. 2. Potential-energy curve for the ground electronic state of H_3^+ and its first-excited singlet electronic state from Ref. 17. The calculated energy of the $1\,^1A'$ state is shifted slightly to conform with the $H^+ + H_2$ ($v = 0$) dissociation asymptote. Vertical arrows suggest transitions at the minimum and maximum photon energies at which photodissociation is observed.

The participation of highly excited vibrational levels in reaction (1) is further supported by the calculated transition dipole moment[17] connecting the ground electronic state with the first-excited singlet state. The oscillator strength is predicted to remain quite high in the asymptotic region with values roughly 40% and 10% of that at the ground-state minimum for H-H_2 separations of 2.1 and 2.9 Å, respectively. This is quite consistent with our probing of a small fractional population of the H_3^+ beam in a fully allowed electronic transition. The relative photofragment yield (Fig. 1) immediately above threshold rises more rapidly than the calculated oscillator strength, suggesting that the fractional population of the vibrational levels in the beam decreases with increasing vibrational excitation, as expected from reaction (2).

In summary, we report here the first observation of the photodissociation of H_3^+ to form H_2^+. We attribute this process to electronic excitation from high rovibrational levels of the ground electronic state to the first-excited singlet state of H_3^+. Substantial verification of the electronic state assignments could be obtained by determining the anisotropy of the photofragment angular distributions with respect to the polarization of the exciting laser. This was not possible in the present experimental configuration, but will be the subject of future investigation.

This work was supported by the Air Force Astronautics Laboratory (Contract No. F04611-87-C-0025). We acknowledge very helpful and stimulating discussions with Dr. H. Helm and Dr. R. P. Saxon, and the technical support of M. Nicholson.

[1]A. Dalgarno and J. H. Black, Rep. Prog. Phys. **39**, 573 (1976).
[2]J. B. A. Mitchell, in *Atomic Processes in Electron-Ion and Ion-Ion Collisions*, edited by F. Brouillard (Plenum, New York, 1986), pp. 185–222.
[3]H. H. Michels and R. H. Hobbs, in *Production and Neutralization of Negative Ions and Beams*, edited by K. Prelec (American Institute of Physics, New York, 1984), pp. 118–124.
[4]T. Oka, in *Molecular Ions: Spectroscopy, Structure, and Chemistry*, edited by T. A. Miller and V. E. Bondybey (North-Holland, Amsterdam, 1983) pp. 73–90.
[5]K. Hirao and S. Yamabe, Chem. Phys. Lett. **80**, 237 (1983).
[6]Y. Yamaguchi, J. F. Gaw, and H. F. Schaefer, J. Chem. Phys. **78**, 4074 (1983).
[7]M. Okumura, L. I. Yeh, and Y. T. Lee, J. Chem. Phys. **83**, 3705 (1985).
[8]T. Oka, Phys. Rev. Lett. **45**, 531 (1980).
[9]J. T. Shy, J. W. Farley, W. E. Lamb, and W. H. Wing, Phys. Rev. Lett. **45**, 535 (1980).
[10]M. J. Gaillard, D. S. Gemmell, G. Goldring, I. Levine, W. J. Bietsch, J. C. Poizat, A. J. Ratkowski, J. Remillieux, Z. Vager, and B. J. Zabransky, Phys. Rev. A **17**, 1797 (1978).
[11]F. Petty and T. F. Moran, Chem. Phys. Lett. **5**, 64 (1970).
[12]A. Carrington and R. A. Kennedy, J. Chem. Phys. **81**, 91 (1984).
[13]J. O. Hirschfelder, J. Chem. Phys. **6**, 795 (1938).
[14]H. Conroy, J. Chem. Phys. **51**, 3979 (1969).
[15]K. Kawaoka and R. F. Borkman, J. Chem. Phys. **54**, 4234 (1971).
[16]L. J. Schaad, and W. V. Hicks, J. Chem. Phys. **61**, 1934 (1974).
[17]D. Talbi and R. Saxon, J. Chem. Phys. **89**, 2235 (1988).
[18]B. Peart and K. T. Dolder, J. Phys. B **7**, 1567 (1974).
[19]Y. K. Bae and P. C. Cosby (unpublished).
[20]T. E. Sharp, At. Data **2**, 119 (1971).
[21]S. Miller and J. Tennyson, J. Mol. Spectrosc. **126**, 183 (1987).
[22]D. L. Smith and J. H. Futrell, J. Phys. B **8**, 803 (1975).
[23]Y. K. Bae, P. C. Cosby, and D. C. Lorents, Chem. Phys. Lett. **159**, 214 (1989).

APPENDIX E

OBSERVATION OF HIGH-LYING VIBRATIONAL PREDISSOCIATION STATES OF H_5^+

OBSERVATION OF HIGH-LYING VIBRATIONAL PREDISSOCIATION STATES OF H_5^+

Young K. Bae
Molecular Physics Laboratory
SRI International
Menlo Park, CA 94025

ABSTRACT

Photodissociation spectrum of H_5^+ between 5,400 and 10,000 cm^{-1} has been measured by monitoring the H_3^+ photofragment yield. Only four vibrational predissociation bands have been observed near 7000 cm^{-1}. The observed bands are broad; their rotational structures were not resolved by the 1 cm^{-1} linewidth of the laser. They are tentatively assigned to overtone and combination bands.

Submitted to Chem. Phys. Lett.

MP 90-049
March 14, 1990

The H_5^+ cluster ion is the first member of the H_{2n+1}^+ cluster ions which are the simplest and most fundamental cluster ions. Ab initio quantum calculations[1] predicted that H_{2n+1}^+ ($n \leq 4$) cluster ions can be approximately described as H_3^+ surrounded by n-1 H_2 molecules. Although the H_5^+ is the simplest among members, theoretical calculations found its structure to deviate the most from the $H_3^+ \bullet H_2$ picture.[1] The calculation[1] also revealed that the global minimum energy geometry is C_{2v}, however, H_5^+ ion is so floppy that there are three more neighboring stationary geometries with significantly different vibrational frequencies.[1]

One way of experimentally investigating the vibrational states of the H_5^+ is measuring its vibrational predissociation spectrum. The H_5^+ has a relatively small dissociation energy into H_3^+ + H_2 which is measured to be approximately 2000 cm^{-1}.[2,3] Thus, upon excitation of vibrational modes having greater energies than the dissociation energy, such as the stretch mode of H_2, the cluster dissociates. By monitoring photofragment yields as a function of excitation energies, vibrational bands of the H_5^+ can be studied. With this method Okumura et al.[4] first identified two *vibrational bands near* 4,000 cm^{-1}. No rotational structures were observed although their laser resolution (0.5 cm^{-1}) was enough to resolve the theoretically estimated rotational intervals 6 to 7 cm^{-1}.[4] They attribute the absence of the rotational structures to homogenious broadening and/or spectral congestion caused by the high internal temperature of the ion. Although their observed frequencies of H_7^+ and H_9^+ agreed well with ab initio predictions, those of H_5^+ did not. In the later work[5] they repeated the measurements with a colder ion source and a higher resolution laser, but still was not able to resolve rotational structures. They identified an additional weak band and assigned the new band to either an overtone and/or combination band. They also searched for other weaker bands up to 5300 cm^{-1} and found no additional features.

I have extended the phodissociation spectrum to 10,000 cm^{-1} and found four new bands clustered around 7000 cm^{-1}. In the measured range no other features have been observed. Details of experimental description is published elsewhere.[6] Briefly, H_5^+ cluster ions were generated by 200-eV electron impact near (~1 mm) the exit of the nozzle of the pulsed supersonic expansion of

room-temperature H_2 gas. Here the H_5^+ ions are formed in the following reactions in the supersonic expansion:

$$H_2 + e \rightarrow H_2^+ + 2e, \quad (1)$$

$$H_2^+ + H_2 \rightarrow H_3^+ + H, \quad (2)$$

and

$$H_3^+ + 2H_2 \rightarrow H_5^+ + H_2. \quad (3)$$

The generated ions were extracted coaxially through a skimmer by a weak (~1 V/cm) electric field, accelerated to 2 keV, mass selected by a 60° magnetic sector, then coaxially interacted with a laser beam over a distance of 60 cm. The mass analyzed and collimated H_5^+ ion beam was composed of 200 μs FWHM pulses with a peak current of 20 nA. Photofragments were energy analyzed by a cylindrical electrostatic energy analyzer and detected by a multichannel plate detector. A significant fraction of H_3^+ fragments resulted from the metastable decay of H_5^+ ions. With the interaction vacuum chamber pressure of 3×10^{-7} Torr, the collisional fragment counts were negligible compared with photofragment and metastable-decay fragment counts. At a laser power of 1 mJ/pulse the ratio of the photofragment counts to the metastable-decay fragment counts at the strongest transition peak was about 6. For each laser shot, both the counts with laser on and off were separately stored in a computer. The relative photofragment yield was obtained by dividing the difference in counts with the laser on and off by the accumulated ion and laser beam intensities. The laser wavelengths between 5400 cm^{-1} and 10,000 cm^{-1} were generated by Raman shifting the YAG pumped dye laser output operating at 10 Hz in 30 atm H_2 gas. The laser was operated synchronously with the pulsed ion beam. Only the second order of the Stokes lines was selected by using four Pellin-Broca prisms and interacted with the ion beam. With this setup, we could practically eliminate the laser beam walk resulting from the angular divergence of the prisms.

In the measured wavelengths region between 5,400 and 10,000 cm^{-1}, H_5^+ was observed to

photodissoiciate only into the $H_3^+ + H_2$ channel. Figure 1 shows a portion of the whole spectrum which shows the four observed bands. Other weaker transitions might exist, however, their oscillator strengths should be an order of magnitude less than the observed ones. The observed bands are all broad with FWHM widths of ~100 cm^{-1}. No rotational structures were resolved although the predicted[4] rotational spacing (6-7 cm^{-1}) is much larger than the laser line width (1 cm^{-1}). Because the rotational structures were not resolved, the band maxima were assigned to band origins. The uncertainties in this assignment resulting from the bandheads and other pileups of lines could be very large. Thus, the following assignments are only tentative.

The observed three vibrational frequencies by Okumura et al. are listed in Table 1.[5] They assigned 3532, 3910, and 4230 cm^{-1} bands to the H_3^+ symmetric stretch band (ν_2), the H_2 stretch band (ν_1), and the combination or overtone band ($\nu_1+\nu_8$ or $3\nu_4$) in H_5^+, respectively. Here the ν_8 is the intermolecular stretch mode between H_3^+ and H_2, and ν_4 is the asymmetric stretch mode of H_3^+ in H_5^+ which was predicted[1] to have a very large oscillator strength. They also suggested that the 3910 cm^{-1} band might be a Fermi resonance of the ν_1 and $\nu_2 + \nu_8$ bands.

Table 1 also lists the four new vibrational frequencies observed in this work. It is surprising to observe only four bands in the whole range of spectrum between 5,400 and 10,000 cm^{-1} because in this range many other overtone and combination bands can be expected. I first noticed that the two stronger bands at 6690 and 7490 cm^{-1} lie close to the possible first overtones of the ν_2 and ν_1 bands observed by Okumura et al. respectively.[4,5] If they are the first overtones of fundamentals, the anharmonic terms, $x_e\omega_e$, for ν_2 and ν_1 modes can be estimated to be ~190 and ~170 cm^{-1} respectively combining the results of this work with those of Okumura et al. (Perhaps for these anharmonic terms it is more appropriate to use the notations for the polyatomic molecules instead of those of diatomic molecules. In this case, $x_{ii}^o=-2x_e\omega_e$.[7] Then, $x_{22}^o=-380$ cm^{-1} and $x_{11}^o=-340$ cm^{-1}.) Accordingly, the scaled harmonic frequencies for the ν_2 and ν_1 modes can be estimated to be ~3910 and ~4250 cm^{-1} respectively. The estimated harmonic frequency 4250 cm^{-1} of the ν_1 mode is close to the CISD level calculated value (4235 cm^{-1}) of the C_{2v}

geometry of Yamaguchi et al.[1] However, the estimated harmonic frequency 3910 cm^{-1} of ν_2 is not in good agreement with any of the calculated values. It is suggestive that the band at 7130 cm^{-1} might be a combination band, $\nu_1 + \nu_2$. This assignment requires the anharmonic term x_{12}^o between ν_1 and ν_2 modes to be --310 cm^{-1}. The 7770 cm^{-1} band might also be a combination band $2\nu_1 + \nu_8$. This implies that around 7,000 cm^{-1} there should be a $2\nu_2 + \nu_8$ band, however, in the measured spectrum its existence is not obvious.

The observed peaks might be broadened by homogenious broadening and/or spectral congestion which is caused by a high internal ro-vibrational temperature of the cluster ion. H_2^+ ions formed in the reaction (1) can have up to several eV of ro-vibraional energies. Furthermore, the reaction (2) is 1.8 eV exoergic, thus a wide range of excited rovibrational states is expected to remain in H_3^+.[8] In fact with the same source Bae and Cosby[9] recently observed a direct photodissociation between very highly excited ground states and the first electronically excited dissociative state. The observation indicated that some portions of the produced H_3^+ ions are vibrationally hot. These vibrationally excited states are presumably not easily quenched in the reaction (3), and consequently the produced H_5^+ ions can be highly excited. The details of transferring mechanism of the excess energy of H_3^+ into internal energy of H_5^+ is not understood. The excess energy in H_5^+ was studied by Kirchner and Bowers[10] by measuring the kinetic energy distribution in metastable decay components with lifetimes of ~10^{-6} μs. They observed substantial populations of their H_5^+ ions are highly ro-vibrationally excited. Relatively large probability was observed even for very high J_0 (up to 29), v = 0. The ions in this work might be relatively colder than theirs, but apparently they still have a high temperature because significant amounts of metastable decay were also observed in this work.

More definitive assignments of observed bands will be possible when more bands and rotational structures are observed. This can be achieved by using a higher power laser and a colder ion source which will substantially reduce the metastable decay rate. Especially, the colder ion source similar to the Corona discharge source used by Okumura et al.[5] will be very useful.

ACKNOWLEDGEMENT

This work was supported by the Air Force Astronautics Laboratory under contract F04611-87-C-0025. We would like thank Mr. M. Dyer for helping to build the Raman cell and Drs. H. Helm and P. C. Cosby for helpful discussions.

REFERENCES

1. Yamaguchi, J. F. Gaw, R. B. Remington, and H. F. Schaefer III, J. Chem. Phys. **86**, 5072 (1987) and references therein.

2. J. Beuhler, S. Ehrenson, and L. Friedman, J. Chem. Phys. **79**, 5982 (1983).

3. T. Elford, J. Chem. Phys. **79**, 5951 (1983).

4. Okumura, L. I. Yeh, and Y. T. Lee, J. Chem. Phys. **83**, 3705 (1985).

5. Okumura, L. I. Yeh, and Y. T. Lee, J. Chem. Phys. **88**, 79 (1988).

6. Bae, M. Nicholson, and P. C. Cosby, submitted to Rev. Sci. Inst.

7. G. Herzberg, F.R.S., Molecular Spectra and Molecular Structure II. (D. Van Nostrand Reinhold Co., Inc., New. York, 1950).

8. B. A. Mitchell, in Atomic Processes in Electron-Ion and Ion-Ion Collisions, edited by F. Brouillard (Plenum. New York, 1986), pp. 185-222.

9. Bae and P. C. Cosby, Phys. Rev. A, **41**, 1741 (1990).

10. J. Kirchner and M. T. Bowers, J. Phys. Chem., **91**, 2573 (1987).

FIGURE CAPTIONS

Figure 1. Vibrational predissociation spectrum of H_5^+ that shows the observed four bands with a laser linewidth 1 cm^{-1}.

TABLE 1

Observed Bands (cm^{-1})	Assignments
3532*	ν_2
3910*	ν_1
4230*	$\nu_1 + \nu_8$ or $3\nu_4$
6690	$2\nu_2$
7130	$\nu_1 + \nu_2$
7490	$2\nu_1$
7770	$2\nu_1 + \nu_8$

* Measured by Okumura, Yeh, and Lee.[5]

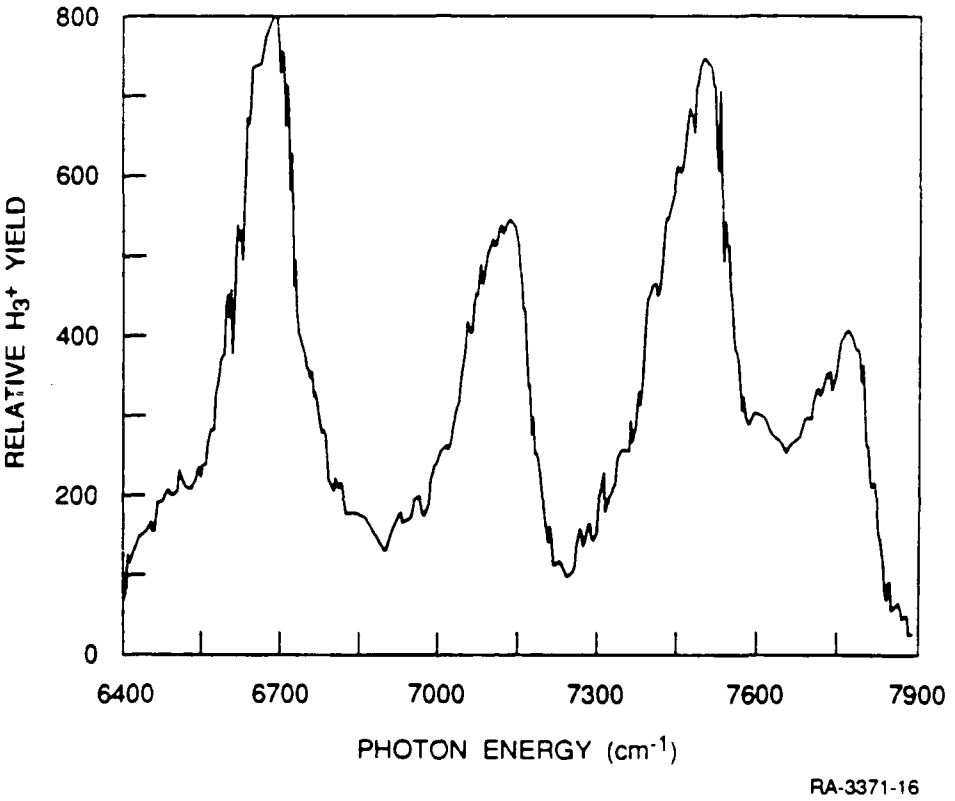
800
600
400
200
0
RELATIVE H_3^+ YIELD
6400
6700
7000
7300
7600
7900
PHOTON ENERGY (cm^{-1})
RA-3371-16